

Monte Carlo Simulations of the Structures and Optical Absorption Spectra of Na Atoms in Ar Clusters, Surfaces, and Solids; a Detailed Presentation of the Theoretical Methods Used

**Jerry A. Boatz
Mario E. Fajardo**

June 1995

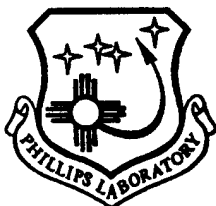
Special Report



APPROVED FOR PUBLIC RELEASE; DISTRIBUTION UNLIMITED.

19950711 012

DTIC QUALITY INSPECTED 5



**PHILLIPS LABORATORY
Propulsion Directorate
AIR FORCE MATERIEL COMMAND
EDWARDS AIR FORCE BASE CA 93524-7048**

NOTICE

When U.S. Government drawings, specifications, or other data are used for any purpose other than a definitely related Government procurement operation, the fact that the Government may have formulated, furnished, or in any way supplied the said drawings, specifications, or other data, is not to be regarded by implication or otherwise, or in any way licensing the holder or any other person or corporation, or conveying any rights or permission to manufacture, use or sell any patented invention that may be related thereto.

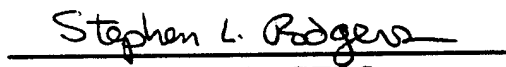
FOREWORD

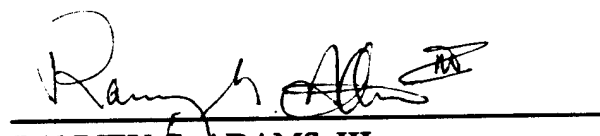
This special technical report was prepared under contract JON: 2303M2C8, for Operating Location AC, Phillips Laboratory, Edwards AFB CA 93524-7001. Project Manager for Phillips Laboratory was Dr. Mario Fajardo.

The report has been reviewed and is approved for release and distribution in accordance with the distribution statement on the cover and on the SF Form 298.

 13JUN95

MARIO E. FAJARDO
Project Manager


STEPHEN L. RODGERS
Director
Fundamental Technologies Division


RANNEY G. ADAMS, III
Public Affairs Director

REPORT DOCUMENTATION PAGE			Form Approved OMB No 0704-0188	
Public reporting burden for this collection of information is estimated to average 1 hour per response, including the time for reviewing instructions searching existing data sources gathering and maintaining the data needed, and completing and reviewing the collection of information. Send comments regarding this burden estimate or any other aspect of this collection of information, including suggestions for reducing this burden to Washington Headquarters Services, Directorate for Information Operations and Reports, 1215 Jefferson Davis Highway, Suite 1204, Arlington, VA 22202-4302, and to the Office of Management and Budget, Paperwork Reduction Project (0740-0188), Washington DC 20503.				
1. AGENCY USE ONLY (LEAVE BLANK)		2. REPORT DATE June 1995		3. REPORT TYPE AND DATES COVERED Special Report
4. TITLE AND SUBTITLE Monte Carlo Simulations of the Structures and Optical Absorption Spectra of Na Atoms in Ar Clusters, Surfaces, and Solids; a Detailed Presentation of the Theoretical Methods Used			5. FUNDING NUMBERS C: PE: 61102F PR: 2303 TA: M2C8	
6. AUTHOR(S) Jerry A. Boatz and Mario E. Fajardo				
7. PERFORMING ORGANIZATION NAME(S) AND ADDRESS(ES) Phillips Laboratory OLAC PL/RKFE 12 Saturn Blvd. Edwards AFB CA 93524-7680			8. PERFORMING ORGANIZATION REPORT NUMBER PL-TR-94-3024	
9. SPONSORING/MONITORING AGENCY NAME(S) AND ADDRESS(ES)			10. SPONSORING/MONITORING AGENCY REPORT NUMBER	
11. SUPPLEMENTARY NOTES COSATI CODE(S): 0702				
12a. DISTRIBUTION/AVAILABILITY STATEMENT Approved for Public Release; Distribution is Unlimited			12b. DISTRIBUTION CODE A	
13. ABSTRACT (MAXIMUM 200 WORDS) Optical absorption spectra of Na/Ar systems are calculated by combining the classical Monte Carlo simulation method with a quantum mechanical first-order perturbation scheme [Balling and Wright, J. Chem. Phys. 79, 2941 (1983)] for estimating the energies of the $\text{Na}^+ 3p(^2P)$ excited states. The model incorporates many drastic approximations, but contains no adjustable parameters. Our Na/Ar matrix simulations generated relaxed structures for several candidate trapping sites based on various sized vacancies in fcc solid Ar. Trapping sites for which the equilibrium structures belong to the O_h or T_d point groups yielded the experimentally well known "triplet" absorption lineshape; for these cases the splitting of the degeneracy of the excited $\text{Na}^+ 3p(^2P)$ state is due solely to fluctuations away from the equilibrium structures. Simulations of Na/Ar clusters, surfaces, and matrix sites possessing a strong permanent axial asymmetry yielded a widely split "doublet plus singlet" absorption lineshape. Despite our success at reproducing several qualitative aspects of the absorption spectroscopy of Na/Ar matrices, our simulations failed to quantitatively reproduce the experimental data. We discuss the major limitations of our model, as well as several possible improvements.				
14. SUBJECT TERMS alkali metal atoms; argon; clusters; high energy density matter; matrix isolation spectroscopy; Monte Carlo simulations; optical absorption; rare gas solids; sodium atoms; surfaces.			15. NUMBER OF PAGES 64	
			16. PRICE CODE	
17. SECURITY CLASSIFICATION OF REPORT Unclassified	18. SECURITY CLASSIFICATION OF THIS PAGE Unclassified	19. SECURITY CLASSIFICATION OF ABSTRACT Unclassified	20. LIMITATION OF ABSTRACT SAR	

TABLE OF CONTENTS

<u>SECTION</u>	<u>PAGE</u>
I. INTRODUCTION	1
II. BACKGROUND	
A. Matrix Experiments	2
B. Absorption Spectra and Trapping Site Models	2
C. Other Useful Perspectives	3
III. THEORY	
A. Fermi's Golden Rule Lineshape Expression	5
B. Transition Dipole Integral	5
C. Summation Over Initial States	7
D. Evaluation of the Lineshape Integral	7
E. Initial and Final State Energies	9
F. Gas-to-Matrix Spectral Shifts	11
IV. METHODOLOGY	
A. Monte Carlo Simulation Method	12
B. Boundary Conditions	13
C. Na-Ar and Ar-Ar Pair Potentials	14
D. Computational Details	16
V. RESULTS	
A. NaAr Diatomic	17
B. Na/Ar Clusters	17
C. Na/Ar Surfaces	22
D. Pure Solid Ar	24
E. Na/Ar Matrices	
1. Finite size effects	24
2. Simulations at $T = 10$ K	35
3. Temperature Effects	37
VI. DISCUSSION	
A. Contributions of the Present Model	39
B. Comparison with Experiments and Previous Models	45
C. Limitations of the Present Model	46
VII. CONCLUSIONS	47
VIII. FUTURE PLANS	48
REFERENCES	49

LIST OF FIGURES

<u>Figure</u>	<u>Caption</u>	<u>Page</u>
1	Na-Ar and Ar-Ar diatomic potential energy curves, and V_{shift}	15
2	Simulated 3s→3p absorption spectra of NaAr _n clusters at T = 1- K, for n=1, 2, 3, 6, 11, and 12	18
3	Simulated RPDF and 3s→3p absorption spectrum of a Na atom on an Ar {111} surface at T = 10 K	23
4	Simulated RPDF and 3s→3p absorption spectrum for a Na atom in a relaxed O _h interstitial site in solid Ar at T = 10 K	26
5	Simulated RPDF and 3s→3p absorption spectrum for a Na atom in a relaxed O _h interstitial site in solid Ar at T = 10 K, <i>after</i> "annealing" to T = 50 K	27
6	Simulated RPDF and 3s→3p absorption spectrum for a Na atom in a relaxed one-atom substitutional site in solid Ar at T = 10 K	28
7	Simulated RPDF and 3s→3p absorption spectrum for a Na atom in a relaxed two-atom vacancy in solid Ar at T = 10 K	29
8	Simulated RPDF and 3s→3p absorption spectrum for a Na atom in a relaxed three-atom vacancy in solid Ar at T = 10 K	30
9	Simulated RPDF and 3s→3p absorption spectrum for a Na atom in a relaxed four-atom vacancy in solid Ar at T = 10 K	31
10	Simulated RPDF and 3s→3p absorption spectrum for a Na atom in a relaxed five-atom vacancy in solid Ar at T = 10 K	32
11	Simulated RPDF and 3s→3p absorption spectrum for a Na atom in a relaxed six-atom vacancy in solid Ar at T = 10 K	33
12	Simulated RPDF and 3s→3p absorption spectrum for a Na atom in a relaxed thirteen-atom vacancy in Solid Ar at T = 10 K	34
13	Temperature dependence of the simulated 3s→3p absorption spectrum for a Na atom in a relaxed O _h interstitial site in solid Ar	38
14	Temperature dependence of the simulated 3s→3p absorption spectrum for a Na atom in a relaxed one-atom substitutional site in solid Ar	40
15	Temperature dependence of the simulated 3s→3p absorption spectrum for a Na atom in a relaxed two-atom substitutional site in solid Ar	41

LIST OF TABLES

<u>Table</u>	<u>Title</u>	<u>Page</u>
1	Summary of optical absorption peaks calculated in this study at T = 10 K	19
2	Summary of results of NaAr _n cluster and Na/Ar surface RPDF simulations at T = 10 K	20
3	Summary of calculated ensemble averaged total ground state energies, $\langle E_1(Q) \rangle_{ave}$, and the contribution from the averaged M-Rg energy, $\langle U_{M-Rg} \rangle_{ave}$, for simulations carried out at T = 10 K	21
4	Summary of results of Na/Ar matrix RPDF simulations at T = 10 K	25
5	Summary of temperature dependence of the optical absorption peaks calculated in this study	42
6	Summary of experimentally observed optical absorptions of Na/Ar matrices	43

Accession For		
NTIS	CRA&I	<input checked="" type="checkbox"/>
DTIC	TAB	<input type="checkbox"/>
Unannounced		<input type="checkbox"/>
Justification _____		
By _____		
Distribution / _____		
Availability Codes		
Dist	Avail and/or Special	
A-1		

I. INTRODUCTION

Considerable advances have been made in the production and understanding of prototypical cryogenic solid propellant systems within the US Air Force High Energy Density Materials (HEDM) program¹. This HEDM effort is motivated by thermochemical estimates of the performance of rocket propellant systems consisting of light energetic atoms trapped in cryogenic solid hydrogen². These preliminary successes demand further improvements in our knowledge of these materials in order to refine our evaluations of propellant system performance. For example, the determination of microscopic trapping site structures would enable estimates of the bulk fuel density, a critical property affecting performance. The simulations described in this manuscript are only part of a broader effort in the HEDM program to apply theoretical chemical methods to issues connected with advanced chemical propellants.

Alkali metal/rare-gas (M/Rg) matrices are nearly perfect model systems for the cryogenic solid propellants under consideration. In particular, Na/Rg matrices have been extensively studied experimentally³⁻¹². Recent experimental efforts in this laboratory have demonstrated the existence of novel, previously unaccessed, trapping sites for Li and Na atoms in Ar and Kr matrices^{13,14}. The majority of these matrix results take the form of optical absorption and emission spectra, and provide an extensive database of experimental results for comparison with theoretical calculations. The Na/Ar system is particularly amenable to theoretical study because of the applicability of classical molecular dynamics and Monte Carlo simulation techniques, and because of the availability of good Na-Ar and Ar-Ar intermolecular potentials¹⁵⁻²¹.

This situation has prompted us to attempt to develop a simple method of connecting the observed matrix isolation spectroscopy to the microscopic metal atom trapping site structures. Because of the relative simplicity and speed of our approach, it can be easily applied to a wide variety of M/Rg systems, hopefully resulting in an improved qualitative understanding of the experimental data. Ultimately, lessons learned from these model systems should benefit more sophisticated efforts to understand solid hydrogen systems with their added complexity (*e.g.*: quantum solid behavior, chemical reactivity). A preliminary report on our Na/Ar work has appeared elsewhere²²; this manuscript includes a detailed presentation of our model, more recent results, and a comparison with our newest experimental data.

II. BACKGROUND

A. Matrix Experiments

We have previously reviewed the experimental techniques for producing metal doped matrices¹³ and the optical properties of these samples^{13,14} elsewhere, only a brief summary will be given here. Na/Ar matrices are typically prepared by co-condensing Na atoms with a large excess of Ar atoms onto a cryogenically cooled substrate held in vacuum. Because of the large oscillator strength of the Na atomic resonance absorption ($3s(^2S) \rightarrow 3p(^2P)$, $\lambda_{\text{gas}} \approx 590 \text{ nm}$), the most common diagnostic technique applied to these matrix samples is optical absorption spectroscopy. The Na atom electronic states are substantially perturbed by the matrix environment, with different trapping sites yielding different characteristic spectra. In fact, each site yields a different so-called "triplet" absorption feature; in Na/Ar matrices the red triplet shows peaks near 578, 588, 595 nm, the blue triplet near 536, 545, 554 nm, and the new violet triplet near 504, 511, 523 nm. Additionally, a strong, broad (FWHM $\approx 1000 \text{ cm}^{-1}$) featureless absorption peaking near 460 nm is sometimes observed in Na/Ar matrices. This so-called "460 nm" absorption has been variously assigned to Na atoms in yet another trapping site, or to Na_2 molecules or larger clusters, or to colloidal Na particles.

B. Absorption Spectra and Trapping Site Models

We have also previously reviewed the existing theoretical efforts to explain and connect the matrix spectra and the metal atom trapping site structures^{13,23}.

The appearance of three peaks in the spectra of $S \rightarrow P$ absorptions in metal-atom/rare-gas (M/Rg) matrices is due to the breaking of the three-fold degeneracy of the excited metal atom P-state by the matrix environment. The various competing models proposed to explain the triplet splitting mechanism fall into one of four classes:

- (1) Crystal field models which invoke a static asymmetry in the equilibrium positions of the atoms comprising the trapping environment²⁴⁻²⁸,
- (2) Dynamic Jahn-Teller (J-T) effect models in trapping sites of high mean symmetry, with only minor spin-orbit (S-O) effects due to the matrix environment^{4,11,29-33},
- (3) Dynamic J-T effect models with large S-O modification by the matrix^{12,34-40},
- (4) M^* -Rg exciplex formation⁴¹.

In evaluating these models, we argued²³ as follows for or against each class: (1) studies invoking Li and Na atoms trapped at or near grain-boundaries^{14,42} emphasize the relevance of asymmetrical equilibrium trapping environments, and hence of the crystal field models, (2) application of the Franck-Condon principle to condensed phases⁴³ suggests that

atom trapping site, (3) the recent observation of a well defined triplet absorption feature in the low atomic number Li/Ne system²³ argues against the importance of external S-O modification effects due to mixing of the M atom P-state with Rg states³⁶, (4) finally, we argued that M*-Rg exciplex formation may influence M/Rg emission spectra^{41,45}, but not absorption spectra. Regardless, each of these models raises interesting issues about the photodynamics of M/Rg systems; we hope to incorporate the best aspects of each into our own model.

Questions concerning M/Rg spectra cannot be separated from questions about the underlying M/Rg trapping site structures. Both unrelaxed and equilibrated proposed trapping structures have been evaluated by calculating the M/Rg system energy using various approximation schemes⁴⁶⁻⁵³. These studies concluded that interstitial sites in close-packed rare gas solids are too small to accept an alkali atom, but that plausible trapping sites can be based on single or multiple substitutional vacancies in such solids. Trapping sites of various equilibrium structure symmetries emerge as likely candidates, supporting both the static- and dynamic-distortion absorption spectra models mentioned above.

C. Other Useful Perspectives

We arrived at our present model after consideration of the strengths and weaknesses of the existing M/Rg absorption spectra models described above. A better appreciation of, and perhaps even improvements to, these models can be gained from studies of different but related systems.

Electronic excitations in solid state systems are typically described in terms of "excitons," or separated electron-hole pairs⁵⁴. Excitons are classified into two limiting cases according to the extent of the electron-hole spatial separation as either: tightly bound Frenkel excitons if the separation is smaller than a lattice constant, or as loosely bound Mott-Wannier excitons if the separation is much larger than a lattice constant. The lowest electronic excitations of M/Rg systems considered in this study are properly treated as tightly-bound Frenkel impurity excitons⁵⁵, whereas higher energy excitations corresponding to M atom Rydberg states should be discussed within the Wannier model^{56,57}. In dilute M/Rg systems, the lowest excitations are localized on the M atom ionic core, justifying their treatment as matrix-perturbed isolated M atom states.

Much of the theoretical formalism previously applied to the optical spectra of M/Rg systems has its roots in the study of F-center defects in alkali-halide crystals (*i.e.*, an electron trapped at a negative ion vacancy)^{43,44,58-62}. For example, the optical absorption spectrum of CsF F-centers displays a triplet feature which is explained by a combination of dynamic J-T and S-O modification effects^{44,58-62}. These studies pointed out the intractability of solving the

and S-O modification effects^{44,58-62}. These studies pointed out the intractability of solving the fully quantum mechanical dynamic J-T problem, and introduced various approximation strategies which nonetheless attempted to include some of the effects of lattice vibrations. Several of these strategies will be adopted in this study; *e.g.*: the "Condon" approximation⁴³, classical Franck-Condon principle^{43,62}, and Monte Carlo integration⁶² (*vide infra*). However, the analogy between the F-center and M/Rg problems must not be overstretched. An electron in an F-center is *not* tightly bound to a central ionic core, rather it is delocalized over several nearest neighbor (NN) ion shells⁵⁹, implying an intermediate case between Frenkel and Wannier excitons. Orthogonalization of the trapped electron's wavefunction to the occupied electronic states of the crystal leads to wild structure in its wavefunction in the neighborhood of the ion nuclei, and thus to large S-O interactions. A closer analogy to the M/Rg case can be made to the spectroscopy of S→P transitions of heavy metal ion impurities in alkali-halide crystals⁶³ in which the optically active electrons *are* tied to a central ion core. Similar theoretical methods, however neglecting S-O coupling modifications, were successfully applied to these systems⁶⁴. Thus, we choose not to incorporate S-O coupling modification effects into our M/Rg absorption model at this time.

From a very different perspective, we have gained insights on how to evaluate the matrix environment perturbations on the M atom electronic states. Studies of gas phase pressure broadening of alkali atom absorptions⁶⁵⁻⁷⁰, and of scattering between S and P-state atoms⁷¹⁻⁷³ provide the connection between generalized perturbations and the familiar adiabatic diatomic M-Rg potentials. This literature also utilizes many of the same approximations for treating separated electronic and nuclear coordinates mentioned above in connection to F-centers, however in systems sufficiently simple to allow quantitative comparisons and evaluations. At higher buffer gas pressures multiple perturber effects become important and questions concerning the additivity of many-body interactions⁶⁷⁻⁷⁰, ubiquitous to condensed phase discussions, begin to appear. Consideration of bound states of gas phase collision complexes leads naturally to the consideration of long-lived MRg_n clusters. Theoretical studies of the structures and spectra of MRg_n clusters have begun to appear in the literature⁷⁴⁻⁷⁸ and have had a strong influence on our own work (see also the very recent calculations of BaAr_n clusters⁷⁹). We also note the close similarities between studies of the electronic transitions of these MRg_n clusters and ongoing investigations of the vibrational spectroscopy of polyatomic molecules in rare gas clusters. Particularly relevant are experimental and theoretical studies of the splitting of the triply degenerate ν_3 vibration of SF₆ in Ar clusters⁸⁰⁻⁸³.

In the following section we will attempt to combine the best parts of existing M/Rg absorption theories with the insights provided from the other solid state, gas phase, and

theoretical treatments of M/Rg systems, we will present our model in some detail. We will begin with a very general formalism for the absorption lineshape, to establish a firm theoretical foundation. We then apply successive levels of approximations to arrive at what we believe is the simplest model capable of qualitatively describing the absorptions of M/Rg systems. We will discuss the specific applicability of these approximations to M/Rg systems throughout our development. We hope that this pedagogical approach will help the reader assess the validity of our model, and facilitate future improvements to it.

III. THEORY

A. Fermi's Golden Rule Lineshape Expression

We begin with the dipole approximation expression for the absorption lineshape, $I(\omega)$, derived from Fermi's Golden Rule of time dependent quantum mechanical perturbation theory^{84,85}:

$$I(\omega) = 3 \sum_a \sum_b (p_a - p_b) |\langle \Psi_b | \mathbf{e} \cdot \boldsymbol{\mu} | \Psi_a \rangle|^2 \delta[(E_b - E_a)/\hbar - \omega] \quad (1)$$

in which: ω is the angular frequency of the applied electromagnetic field; p_a and p_b are the probabilities that the system is in its initial and final states -- Ψ_a and Ψ_b -- with energies E_a and E_b , respectively; \mathbf{e} is the unit vector along the electric component of the applied field; $\boldsymbol{\mu}$ is the total dipole moment operator for the system; and the Dirac delta function serves to conserve energy. We now proceed (following Lax⁴³) to evaluate the different constituents of this equation.

B. Transition Dipole Integral

We assume Born-Oppenheimer separable wavefunctions of the form

$$\Psi_a(\mathbf{q}, \mathbf{Q}) = \chi_i(\mathbf{q}) \psi_{im}(\mathbf{Q}) \quad (2)$$

where: i and m specifically label the electronic and vibrational wavefunctions for the initial states, and f and n similarly label the final states. We make the Condon approximation⁴³ that the dependence of the transition dipole integrals on the nuclear coordinates, \mathbf{Q} , may be neglected, thus:

$$I(\omega) = 3 \sum_{i,m} \sum_{f,n} (p_{im} - p_{fn}) |\overline{\mu}_{fn}^{el}|^2 |\langle \psi_{fn}(\mathbf{Q}) | \psi_{im}(\mathbf{Q}) \rangle|^2 \delta[(E_{fn} - E_{im})/\hbar - \omega] \quad (3)$$

in which: $\overline{\mu_n^{el}}$ is the electronic transition moment coupling states χ_i and χ_f , averaged over the nuclear coordinates. The Condon approximation has been shown to hold to within a few percent for the $X(^2\Sigma) \rightarrow A(^2\Pi)$ and $X(^2\Sigma) \rightarrow B(^2\Sigma)$ transitions of the Na-Ar diatomic system by *ab-initio* quantum chemical calculations¹⁶, and we expect similar behavior for the corresponding lowest excitations in larger Na/Ar systems.

The Franck-Condon (F-C) factors can be approximated by using the closure relationship

$$\sum_n |\psi_{fn}(Q)\rangle \langle \psi_{fn}(Q')| = \delta(Q - Q') \quad (4)$$

to evaluate the summation over the final state vibrational wavefunctions, and then using the resulting delta function to evaluate one of the two integrals over nuclear coordinates in Eq. 3. Making use of Eq. 4 also requires that we replace the final state energies, E_{fn} , in the delta function from Eq. 3 with an approximate value, which we take to be the energy at the classical turning points for the final state, Q_T :

$$E_{fn} - E_{im} \rightarrow E_f(Q_T) - E_{im} \equiv \Delta E_{fim}(Q_T). \quad (5)$$

This approximation effectively replaces the summation over overlap integrals in Eq. 3 with an integration over the initial state probability distributions in the nuclear coordinates:

$$I(\omega) = 3 \sum_{i,m} \sum_f (p_{im} - p_f) |\overline{\mu_n^{el}}|^2 \int dQ |\psi_{im}(Q)|^2 \delta[\Delta E_{fim}(Q_T)/\hbar - \omega]. \quad (6)$$

This approach is also formally equivalent to the so-called reflection approximation⁸⁶⁻⁸⁹ to the F-C factors, which is usually applied to bound \rightarrow free transitions, but can be generalized to include bound \rightarrow bound transitions⁸⁷. In fact, this method can yield a surprisingly good approximation of the F-C envelope even for bound \rightarrow bound transitions of diatomic molecules⁹⁰.

C. Summation Over Initial States

For absorption simulations in cryogenic M/Rg systems exposed to weak optical fields we can ignore the final electronic state populations:

$$(p_{im} - p_f) \approx p_{im} . \quad (7)$$

We note that the quantum statistical mechanical ensemble average of a quantity, X , is given by⁸⁵:

$$\langle X \rangle_{ave} = \sum_{\alpha} p_{\alpha} X_{\alpha} . \quad (8)$$

We assume that the M/Rg system is initially in thermodynamic equilibrium, and define the configuration space probability distributions for the initial states, $\rho_i(\mathbf{Q})$, as:

$$p_i \rho_i(\mathbf{Q}) \equiv \sum_m p_{im} |\psi_{im}(\mathbf{Q})|^2 = \langle |\psi_i(\mathbf{Q})|^2 \rangle_{ave} . \quad (9)$$

in which p_i is the probability of finding the system in initial electronic state i . Applying this identification to the expression for the absorption lineshape, yields:

$$I(\omega) = 3 \sum_i \sum_f p_i |\overline{\mu_{if}}|^2 \int d\mathbf{Q} \rho_i(\mathbf{Q}) \delta[\Delta E_{if}(\mathbf{Q}_T)/\hbar - \omega] \quad (10)$$

where we have also further approximated the initial state energies, E_{im} , by the energy of state, I , in the particular nuclear configurations corresponding to the excited state turning points, $E_i(\mathbf{Q}_T)$.

D. Evaluation of the Lineshape Integral

Our Eq. 10 is given in Lax's work (and elsewhere) as the final form of the so-called Semiclassical Franck-Condon lineshape expression, in which the integration over each initial state probability distribution, $\rho_i(\mathbf{Q})$, is to be performed using quantum statistical mechanics. However, more detailed analyses^{87,88,91} point out that in order to evaluate the spatial integration specified by Eq. 10, we must first (in the language of the reflection approximation) properly "normalize" the delta function, or equivalently: convert its argument from angular frequencies to spatial configurations⁹¹. In one-dimension this is easily accomplished by making the substitution⁹²:

$$\delta[f(x)] \rightarrow \sum_j \frac{\delta(x - x_j)}{|f'(x_j)|} \quad (11)$$

where $f'(x)$ is the derivative of $f(x)$ and the x_j are the simple zeros of $f(x)$ such that: $f(x_j) = 0$ and $f'(x_j) \neq 0$. We generalize this substitution to the present multi-dimensional case by replacing:

$$\delta[\Delta E_{\text{fi}}(\mathbf{Q}_T)/\hbar - \omega] \rightarrow \hbar \int_{\{\mathbf{Q}_T\}} \|\bar{\nabla}[\Delta E_{\text{fi}}(\mathbf{Q}_T)]\|^{-1} \delta(\mathbf{Q} - \mathbf{Q}_T) \quad (12)$$

in which we have substituted the (non-zero) norm of the gradient of the energy difference function for the one-dimensional total derivative in Eq. 11. In general for an n -dimensional configuration space, the locus of turning points, $\{\mathbf{Q}_T\}$, will take the form of a number of disconnected, open or closed, $n-1$ dimensional regions. We drop the superfluous explicit integration over the set of turning points appearing in Eq. 12, and make the substitution for the delta function in Eq. 10 to yield the final form of our lineshape expression:

$$I(\omega) = 3\hbar \sum_i \sum_f p_i |\overline{\mu_{\text{fi}}^{\text{el}}}|^2 \int d\mathbf{Q} \rho_i(\mathbf{Q}) \|\bar{\nabla}[\Delta E_{\text{fi}}(\mathbf{Q}_T)]\|^{-1} \delta(\mathbf{Q} - \mathbf{Q}_T). \quad (13)$$

Two major obstacles remain to be resolved in our calculation of the absorption lineshape. Firstly, a systematic evaluation of Eq. 13 might proceed by inverting the transition energy function, $\Delta E_{\text{fi}}(\mathbf{Q}_T) - \hbar\omega$, to yield the complete set of integration points $\{\mathbf{Q}_T\}$ corresponding to each value of ω ; at best a tedious, and perhaps a badly posed task. We will avoid this problem by employing a numerical integration technique (*vide infra*) in which the calculation of the initial state probability distribution, $\rho_i(\mathbf{Q})$, is performed using classical statistical methods. The transition energies for each of the relevant configurations can then be calculated and their contributions to the spectrum weighted by $\rho_i(\mathbf{Q})$, yielding the absorption lineshape in the Classical Franck-Condon Principle limit⁴³. More seriously, careful consideration must be given to the classical divergences arising from integration near possible stationary points where $\bar{\nabla}[\Delta E_{\text{fi}}(\mathbf{Q}_T)] = \vec{0}$. *In this manuscript we avoid these possible unphysical divergences in Eq. 13 by assuming $\|\bar{\nabla}[\Delta E_{\text{fi}}(\mathbf{Q}_T)]\|$ to be constant throughout our simulations.* A more critical analysis of the conditions under which this approximation is justified will appear in a future manuscript by another group⁹³.

E. Initial and Final State Energies

For S→P transitions of M/Rg systems, both the initial M atom electronic state and the rare gas perturbers have spherical symmetry. We will assume that the initial state energy for a given nuclear configuration, $E_i(\mathbf{Q})$, can be calculated as a simple pair-wise sum over the Σ symmetry diatomic potentials:

$$E_i(\mathbf{Q}) = U_{\text{M-Rg}} + U_{\text{Rg-Rg}} = \sum_k V_{\text{M-Rg}}(|\vec{\mathbf{R}}_k|) + \sum_k \sum_{l < k} V_{\text{Rg-Rg}}(|\vec{\mathbf{R}}_l - \vec{\mathbf{R}}_k|) \quad (14)$$

where: $U_{\text{M-Rg}}$ is the contribution due to M-Rg interactions, $U_{\text{Rg-Rg}}$ is the contribution due to Rg-Rg interactions, the indices k and l run over the Rg atoms, the coordinate system is centered on the M atom nucleus, and the zero of energy is defined at infinite separation of all atoms.

For the excited M^* atom P-state interacting with S-state Rg atoms, there are both Σ and Π symmetry diatomic interactions involved, hence a simple angle-independent pairwise summation will not yield the desired M^*/Rg energies. However, following the pioneering work of Baylis⁶⁷, Balling and Wright⁵¹ (henceforth B&W), and independently Sando, Erickson, and Binning⁶⁹, developed a simple and elegant approximation to the M^*/Rg energies based on the assumption of additive *perturbations* to the M^* states due to multiple Rg perturbers. We have repeated B&W's derivation and reproduce it here for convenience, and in order to present the results in a somewhat different format, and also to correct a minor (arithmetical or typographical) error.

We adopt B&W's notation with minor modifications to avoid possible confusion with previously introduced symbols. The Hamiltonian for the M atom optically active electron is:

$$H = H_A(\vec{\mathbf{r}}) + \sum_k V(\vec{\mathbf{r}}, \vec{\mathbf{R}}_k) \quad (15)$$

where $H_A(\vec{\mathbf{r}})$ is the unperturbed Hamiltonian, $V(\vec{\mathbf{r}}, \vec{\mathbf{R}}_k)$ is the perturbation due to the k th Rg atom, and $\vec{\mathbf{r}}$ and $\vec{\mathbf{R}}_k$ are the electronic and nuclear coordinates, respectively, measured from the M atom nucleus. The eigenvalues and eigenfunctions of $H_A(\vec{\mathbf{r}})$ are denoted by ϵ_α and $\chi_\alpha(\vec{\mathbf{r}})$. The eigenvalues, E , of the total Hamiltonian, H , are obtained from first-order degenerate perturbation theory by solving:

$$\det | V_{\alpha\beta} - (E - \epsilon_\alpha) \delta_{\alpha\beta} | = 0 \quad (16)$$

where

$$V_{\alpha\beta} = \sum_k \langle \chi_\alpha(\vec{r}) | V(\vec{r}, \vec{R}_k) | \chi_\beta(\vec{r}) \rangle. \quad (17)$$

For a light alkali M atom P-state, spin-orbit coupling is ignored, and the basis set $\{\chi_\alpha\}$ is restricted to the three free atom states: $\{p_{-1}, p_0, p_1\}$.

B&W proceed by expanding the perturbations in Legendre polynomials (see also Ref. 94):

$$V(\vec{r}, \vec{R}_k) = \sum_L V_L(r, R_k) P_L(\hat{r}, \hat{R}_k) \quad (18)$$

in which r is the magnitude, and \hat{r} the direction of \vec{r} , respectively. Since the angular dependence of the p-state basis functions is represented by $l = 1$ spherical harmonics, $Y_{1m}(\hat{r})$, only the $L = 0$ and $L = 2$ matrix elements survive:

$$V_{\alpha\beta} = \sum_k [\langle \chi_\alpha(r) | V_0(r, R_k) | \chi_\beta(r) \rangle \langle Y_{1\alpha}(r) | P_0(\hat{r}, \hat{R}_k) | Y_{1\beta}(r) \rangle + \langle \chi_\alpha(r) | V_2(r, R_k) | \chi_\beta(r) \rangle \langle Y_{1\alpha}(r) | P_2(\hat{r}, \hat{R}_k) | Y_{1\beta}(r) \rangle]. \quad (19)$$

After applying the spherical harmonic addition theorem⁹⁵ and performing some angular momentum arithmetic⁹⁶, the perturbation matrix becomes:

$$\underline{V} = \sum_k \left(\langle V_0(R_k) \rangle \underline{I} + \frac{1}{10} \langle V_2(R_k) \rangle \begin{Bmatrix} -(3 \cos^2 \theta_k - 1) & -3\sqrt{2} \sin \theta_k \cos \theta_k e^{-i\phi_k} & -3 \sin^2 \theta_k e^{-2i\phi_k} \\ -3\sqrt{2} \sin \theta_k \cos \theta_k e^{i\phi_k} & 2(3 \cos^2 \theta_k - 1) & 3\sqrt{2} \sin \theta_k \cos \theta_k e^{-i\phi_k} \\ -3 \sin^2 \theta_k e^{2i\phi_k} & 3\sqrt{2} \sin \theta_k \cos \theta_k e^{i\phi_k} & -(3 \cos^2 \theta_k - 1) \end{Bmatrix} \right) \quad (20)$$

where⁷¹⁻⁷³:

$$\langle V_0(R_k) \rangle \equiv \langle \chi_\alpha(r) | V_0(r, R_k) | \chi_\beta(r) \rangle = \frac{1}{3} (V_{B\Sigma}(R_k) + 2V_{A\Pi}(R_k)) \quad (21a)$$

$$\langle V_2(R_k) \rangle \equiv \langle \chi_\alpha(r) | V_2(r, R_k) | \chi_\beta(r) \rangle = \frac{5}{3} (V_{B\Sigma}(R_k) - V_{A\Pi}(R_k)). \quad (21b)$$

Combining Eq. 20 and Eq. 21 yields B&W's results, except that we believe that their Eq. 9d for V_{13} contains a multiplicative sign error (see Results Section).

With the present basis set, Eq. 16 will yield up to three distinct energies, E , which represent the contribution to the total energy due to the electronic excitation and the M^*-R_g interactions. These energies can be summed with $U_{R_g-R_g}$ defined in Eq. 14 to give the total system energies for the final states:

$$E_f(Q) = E + U_{R_g-R_g} \quad (22)$$

The M/R_g $S \rightarrow P$ transition energies are calculated as the difference between final and initial state energies, and so the initial and final state R_g-R_g interactions cancel:

$$\hbar\omega_{fi} = E_f(Q) - E_i(Q) = E - U_{M-R_g} \quad (23)$$

F. Gas-to-Matrix Spectral Shifts

We prefer our form of Eq. 20 for the perturbation matrix since each of the terms has a simple physical significance. The term containing $\langle V_0(R_k) \rangle$ represents a pure shift in the excited state energies due to the presence of the perturbors, while the term containing $\langle V_2(R_k) \rangle$ accounts for any splitting of the initial degeneracies. We can make use of this separation to derive a simple expression for the shift of the centroid of the $S \rightarrow P$ absorption band. Since both the initial state U_{M-R_g} term, and the final state term containing $\langle V_0(R_k) \rangle$ depend only on the *magnitudes* of the separations between the M and R_g atoms, recalling Eq. 8 we can write:

$$\begin{aligned}
\langle h\omega_{fi} - \epsilon_{\alpha} \rangle_{ave} &= \langle \left(\sum_k \langle V_0(R_k) \rangle \right) - U_{M-Rg} \rangle_{ave} \\
&= \langle \sum_k [\langle V_0(R_k) \rangle - V_{X\Sigma}(R_k)] \rangle_{ave} \equiv \langle \sum_k V_{shift}(R_k) \rangle_{ave}
\end{aligned} \tag{24}$$

which is simply the difference between the spherically averaged excited state M*-Rg interactions and the ground state M-Rg interactions, averaged over the thermally accessible M-Rg separations; we denote this difference potential by $V_{shift}(R_k)$. For fairly rigid M/Rg structures in which all the atoms have well defined equilibrium positions, the summation and ensemble averages in Eq. 24 can be interchanged, and the centroid shift approximated by:

$$\langle h\omega_{fi} - \epsilon_{\alpha} \rangle_{ave} \approx \sum_k V_{shift}(\langle R_k \rangle_{ave}) \tag{25}$$

where the $\langle R_k \rangle_{ave}$ are the equilibrium M-Rg separations.

To summarize: we have combined approximate expressions for the absorption lineshape, and for estimating the initial and final state energies, to yield a workable model of the absorption spectra of M/Rg systems. Although many severe approximations have been made, the model contains no adjustable parameters and remains general enough to be applied to gas, liquid, and solid phase systems, as well as to clusters and surfaces. More specifically, by including contributions from all thermally accessible nuclear configurations, this model includes some of the effects of fluctuations around relaxed, minimum energy mean structures, and thus combines aspects of both the static crystal field and dynamic J-T models mentioned before. In the following section, we select a specific method of generating the configurations required to perform the ensemble averages, and list some of the relevant details concerning its implementation.

IV. METHODOLOGY

A. Monte Carlo Simulation Method

We have chosen to perform the integration over initial state configurations specified in Eq. 13 by using the classical Monte Carlo (MC) simulation technique. The MC scheme used in this study is based on the original Metropolis algorithm⁹⁷, and our implementation was described in a recent manuscript on Li atom doped Ne solids⁵³. Briefly: the essence of the MC approach is to approximate the true thermodynamic average of some property of interest by an average calculated over a finite sequence of configurations of a small ensemble of atoms. Each subsequent configuration is generated from its predecessor by random displacement of one of the atoms in the ensemble; new configurations are accepted at

random, weighted by a Boltzmann factor of the energy difference between the configurations:

$$P_{\text{accept}} = \exp\{-[E_i^{\text{new}}(Q') - E_i^{\text{old}}(Q)]/k_B T\} \quad (26)$$

where T is the absolute temperature of the ensemble, and k_B is Boltzmann's constant. If $E_i^{\text{new}}(Q') - E_i^{\text{old}}(Q)$ is negative, then the new configuration is automatically accepted. If a proposed configuration is not accepted, the previous one is kept for the averaging process. The work of Metropolis, *et al*, demonstrated that, if the atoms are constrained to be in a box of finite volume, that the ensemble will approach a canonical distribution (N , V , T fixed) in the limit of an infinite sequence of configurations.

B. Boundary Conditions

A MC simulation begins with the choice of an initial configuration for the M and R_g atoms, and may require the specification of boundary conditions for constrained systems. For our Na/Ar matrix simulations, the initial structures were based on an octahedral interstitial site, and on one, two, three, four, five, six, and thirteen-atom vacancies in an otherwise perfect fcc Ar crystal. We also ran simulations of the structure of pure solid Ar to test the procedure. In this study we will restrict our attention to these idealized archetypal trapping sites, and leave simulations of Na atoms in amorphous matrices and rare gas liquids for future efforts.

We used two different size "cells" in the various matrix simulations; one is a roughly cubical arrangement of $6 \times 6 \times 6$ {100} planes containing 108 atoms, the other a similar $8 \times 8 \times 8$ plane collection totaling 256 atoms. These cells are "building blocks" from which an fcc lattice can be generated by repetitive stacking. We used three dimensional periodic boundary conditions⁹⁸ to simulate the infinite solid. The size of the periodic box containing the atoms determines their separations and the density of the solid. In our simulations we used experimental values⁹⁹ of the temperature dependent solid Ar lattice constant, a . We also truncated all interaction potentials and calculations of structural properties for internuclear separations greater than half of the length of a cell edge (*e.g.*: $R_{\text{cutoff}} = 7.97 \text{ \AA}$ for the $6 \times 6 \times 6$ cell, and $R_{\text{cutoff}} = 10.62 \text{ \AA}$ for the $8 \times 8 \times 8$ cell, at $T = 10 \text{ K}$). This truncation scheme requires the inclusion of consistent long-range corrections to the calculated total energies and spectral shifts¹⁰⁰. The missing long range summations are approximated by integration over a mean density of perturbers:

$$E_{\text{corr}} = 4 \pi \rho_{\text{Ar}} \int_{R_{\text{cutoff}}}^{\infty} V(R) R^2 dR \quad (27)$$

in which ρ_{Ar} is the number density of Ar atoms in solid Ar, and $V(R)$ represents $V_{\text{M-Rg}}$, $V_{\text{Rg-Rg}}$, or V_{shift} , depending on which correction is desired. These corrections were not included in our previous work²², and have the unfortunate effect of worsening the quantitative agreement between our results and the experimental data (*vide infra*).

For the Ar surface simulations, the ensemble consisted of six close packed {111} planes, each containing 36 Ar atoms, stacked to yield a small chunk of fcc Ar; the Na atom was placed on an outer close packed surface. We used two-dimensional periodic boundary conditions to mimic an extended surface, and we allowed the structure to relax along the surface normal direction. We neglected any long range corrections, and did not attempt to include any effects of surface roughness in these simulations.

For our simulations of NaAr_n clusters, the initial Ar atom positions were those for a one-atom substitutional vacancy in fcc Ar, with the Na atom at the "center" (only for the NaAr_{13} case was the Na atom actually initially surrounded by Ar atoms).

C. Na-Ar and Ar-Ar Pair Potentials

Both the calculations of the transition energies, Eq. 23, and of the MC configuration acceptance probabilities, Eq. 26, rely on the use of Na-Ar and Ar-Ar pair potentials. The Ar-Ar ground-state potential (HFD-B2, Ref. 21) used in these simulations has been constructed to accurately reproduce spectroscopic, scattering, and bulk data, and is expected to be very reliable. For the Na-Ar interactions, we chose to use the internally consistent set of Na-Ar $X(^2\Sigma)$, $A(^2\Pi)$, and $B(^2\Sigma)$ potentials calculated by Saxon, *et al*¹⁶. The Na-Ar potentials were interpolated using a cubic spline on 0.01 Å intervals. We consider the quantitative discrepancies between these potentials and the published experimental potentials^{15,17-20} to be relatively unimportant to our application, in view of the simplifying approximations we have introduced into our model. We set the asymptotic energy of the

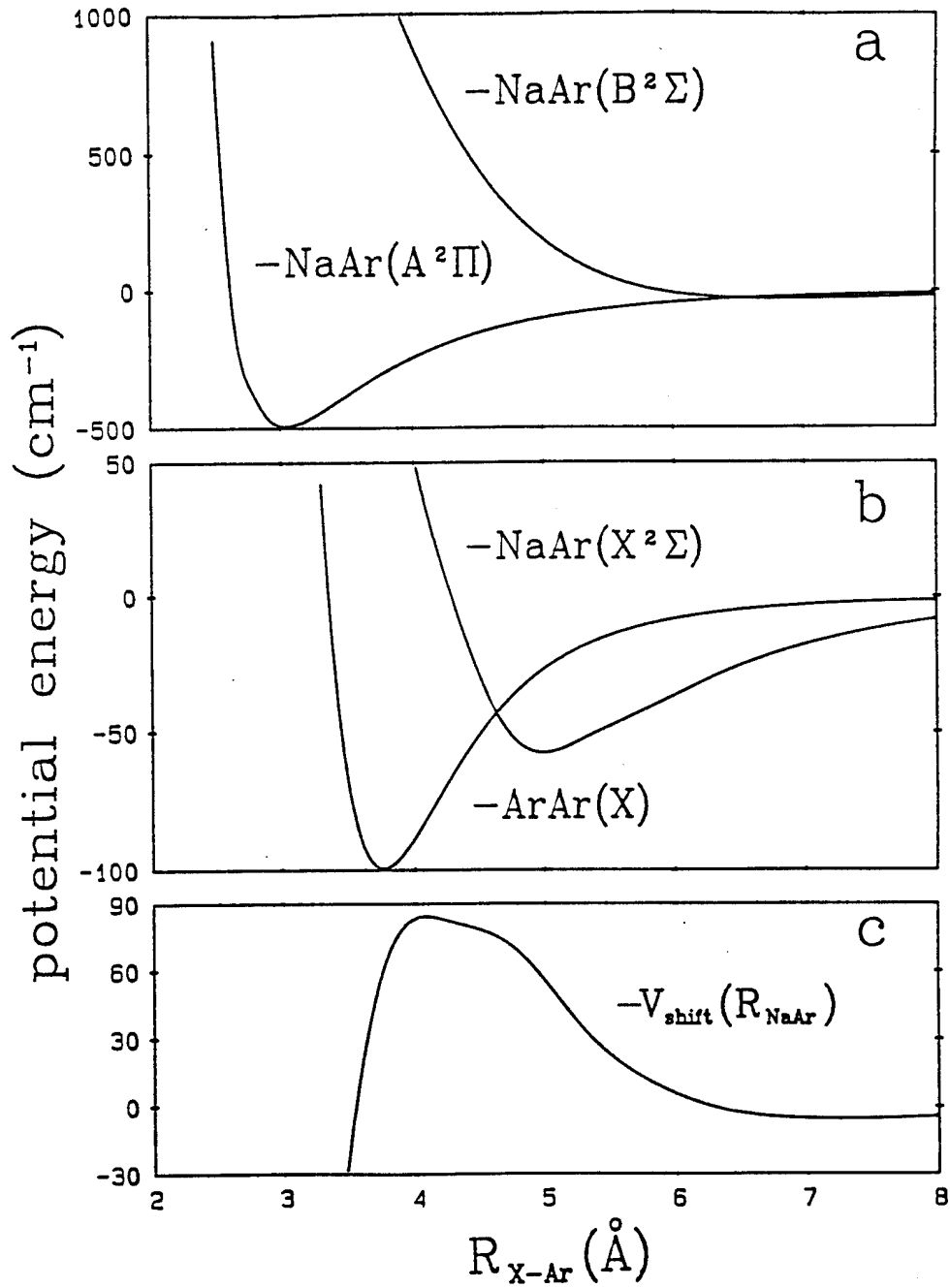


FIG. 1. Na-Ar and Ar-Ar diatomic potential energy curves, and V_{shift} . Panel (a) shows the two lowest $Na^*(3p^2P)$ -Ar excited-state potentials; the asymptotic energy is set to 16968 cm^{-1} in the spectral simulations. Panel (b) shows the ground state Ar-Ar potential ($R_e = 3.76$ Å, $D_e = 100$ cm^{-1}) and the Na-Ar ground state potential ($R_e = 5.01$ Å, $D_e = 55$ cm^{-1}). Panel (c) shows the difference potential, V_{shift} , defined in Eq. 24. The Na-Ar potentials are taken from Ref. 16, and the Ar-Ar potential from Ref. 21.

excited Na*-Ar potentials, ϵ_α from Eq. 16, to 16968 cm⁻¹, the weighted average of the energies of the Na* $2P_{1/2}$ and $2P_{3/2}$ states¹⁰¹. Fig. 1 shows the various Na-Ar and Ar-Ar potentials used in the simulations, as well as the excited-state/ground-state difference potential, V_{shift} , defined above in Eq. 24.

D. Computational Details

As described above, each simulation begins with an ensemble in an artificial, non-equilibrium configuration. We monitor the ensemble's relaxation towards an equilibrium structure by recording values of the total ground state energy, $E_t(Q)$. Precipitous drops in $E_t(Q)$ correspond to abrupt structural rearrangements; eventually $E_t(Q)$ levels off and fluctuates around some value that is characteristic of a particular local minimum energy mean structure. There is in general no *a priori* way of knowing when the system has found the global minimum region of configuration space, hence there is no guarantee that fully relaxed equilibrium structures are being simulated. We mention briefly some of the difficulties we encountered along these lines during our Na/Ar matrix simulations in the Results section, below. Nonetheless, the value of $E_t(Q)$ does serve as a diagnostic of the stability of the system in a particular region of configuration space, so that the averaging process can be carried out over a single mean structure. *Caveat*: subtle isomerizations, common in the NaAr_n cluster simulations, may be more difficult to identify than this statement suggests⁷⁴.

Typical choices of computational parameters are as follows: The maximum distance that an atom is allowed to "hop" in an attempt to reach a new configuration was chosen to yield a 40 to 60% acceptance rate of new configurations. For the matrix, cluster, and surface simulations at temperatures between 10 and 50 K, this hop size is about ± 0.1 Å in each Cartesian coordinate. Each simulation ran for approximately 50,000 "cycles" where each atom is given one opportunity to hop per cycle. Thus, the total number of configurations generated is 50,000 times the number of atoms in the ensemble.

In addition to the absorption lineshape, we also calculate the Na-Ar radial distribution function (RDF or "g(R)") for a given mean structure. The Na-Ar RDF measures the probability of finding an Ar atom at a given distance from the Na atom, relative to the same probability calculated for an ideal Na/Ar gas at the same mean density^{85,100}. We actually prefer to work with the radial *probability* distribution function (RPDF), defined as:

$$\text{RPDF} \equiv 4 \pi R^2 g(R) dR \quad (28)$$

which gives the probability of finding an Ar atom in the interval R to $R + dR$ from the Na atom. We calculate the RPDFs directly as histograms by rounding the Na-Ar distances to the nearest 0.01 Å and binning the contributions. The absorption lineshapes are calculated similarly, by binning the transition energies from Eq. 23 with a resolution of 15 cm⁻¹. Averaging of the RPDFs and of the absorption lineshapes begins only after the first 10 to 20% of the configurations have been generated and discarded. Contributions to the averages are calculated at the end of each cycle. Other useful diagnostics are "snapshot" records of the atomic positions at the beginning and end of the averaging process, as well as the calculated average positions.

V. RESULTS

A. NaAr Diatomic

The simplest Na/Ar system provides the opportunity to test certain aspects of our model and its computer code implementation. We confirmed that the excited state energies calculated from Eq. 16 for a single Ar atom perturber at an arbitrary position agreed numerically with the Na-Ar A(²Π) and B(²Σ) potentials input into the calculation. Similar calculations using the original Balling and Wright Eq. 9d failed this test, confirming the presence of an arithmetical or typographical error.

We also compared the classical NaAr RPDF calculated at $T = 10$ K with the square of the ground state NaAr vibrational wavefunction calculated by numerical integration^{102,103} of the one-dimensional radial Schroedinger equation for the Na-Ar X(²Σ) potential. The quantum ground state Na-Ar probability distribution peaks at 5.08 Å and has a full width at half maximum (FWHM) of 0.71 Å; our calculated classical distribution peaks at 4.99 Å, with a FWHM of 0.55 Å. Thus, in this case our classical method at $T = 10$ K underpredicts the spread of positions available to the system even at $T = 0$ K, and should therefore also underpredict the width and splitting of the absorption lineshape. This systematic error most likely pervades all of our Na/Ar cluster, surface, and matrix calculations.

B. Na/Ar Clusters

Fig. 2 shows the absorption spectra of NaAr_n clusters containing one, two, three, six, 11, and 12 Ar atoms, at $T = 10$ K. Table 1 includes the absorption peak positions, as well as the calculated peak shifts from the free Na atom transition energy. We do not show the corresponding Na-Ar RPDFs, but Table 2 contains a summary of the RPDF peak positions, the number of Ar atoms in each peak, and the equilibrium structure symmetry for the entire cluster. The calculated equilibrium structures correspond to nearly close-packed Ar clusters

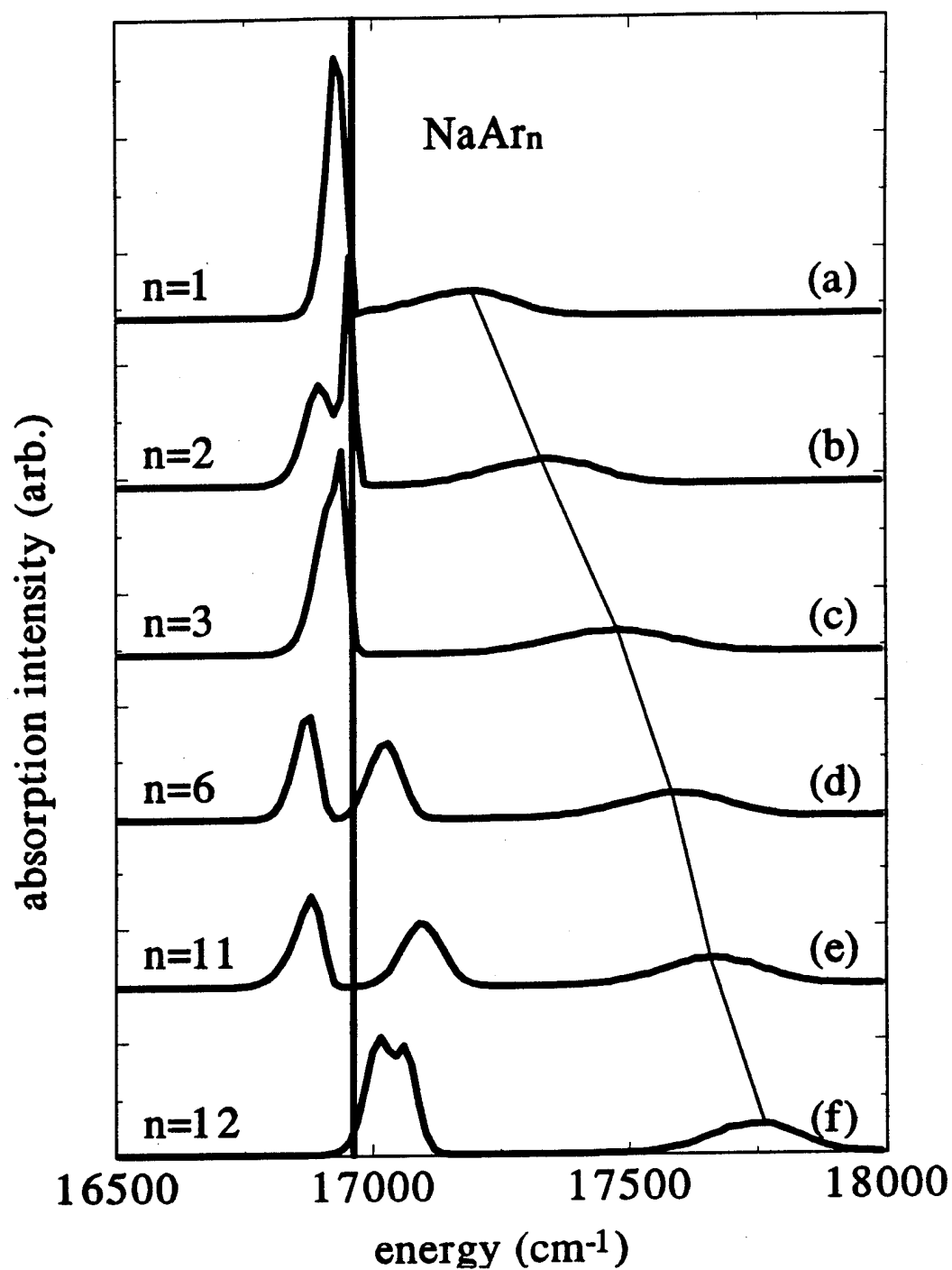


FIG. 2. Simulated 3s→3p absorption spectra of NaAr_n clusters at T = 10 K, for n=1, 2, 3, 6, 11, and 12. The vertical thick line shows the position of the free Na* atom absorption centered at 16968 cm⁻¹. The slanting thin line shows the shift in the peak of the blue n-perturber satellite absorption.

Table 1. Summary of optical absorption peaks calculated in this study at $T = 10$ K. Peak positions are rounded to the nearest 15 cm^{-1} , and shifts from the free Na atom $3s(^2S) \rightarrow 3p(^2P)$ transitions centered around 16968 cm^{-1} are rounded to the nearest 5 cm^{-1} . The matrix site values are from simulations employing the $6 \times 6 \times 6 \{100\}$ plane cell and include a long range cutoff correction of -210 cm^{-1} .

<u>system</u>	<u>absorption peak energies (cm^{-1})</u>	<u>peak shifts from free Na atom (cm^{-1})</u>	<u>centroid shift (cm^{-1})</u>
clusters:			
NaAr	16925, 17195	-45, +225	+130
NaAr ₂	16895, 16955, 17330	-75, -15, +360	+180
NaAr ₃	16940, 17480	-30, +510	+220
NaAr ₆	16880, 17030, 17585	-90, +60, +615	+280
NaAr ₁₁	16880, 17090, 17660	-90, +120, +690	+330
NaAr ₁₂	17015, 17060, 17765	+45, +90, +795	+390
surface site:	16775, 17720	-195, +750	+210
matrix sites:			
O _h interstitial	17540, 17675, 18155	+570, +705, +1185	+805
O _h int. annealed	17585, 17810, 17975	+615, +840, +1005	+820
1-atom subst.	17630, 17765, 17930	+660, +795, +960	+800
2-atom subst.	15770, 18455, 18770	-1200, +1485, +1800	+690
3-atom subst.	16745, 16985, 19325	-225, +15, +2355	+715
4-atom subst.	17540, 17645, 17765	+570, +675, +795	+680
5-atom subst.	17150, 17705, 17840	+180, +735, +870	+600
6-atom subst.	17360, 17435, 17510	+390, +465, +540	+465
13-atom subst.	16955	-15	-15

Table 2. Summary of results of the NaAr_n cluster and Na/Ar surface RPDF simulations at $T = 10$ K. The first entry gives the position of a peak maximum in the RPDF; the second entry gives the mean position calculated over the entire peak, and the number of Ar atoms in that peak. For the cluster simulations, the last column lists the symmetry point group of the entire cluster.

		RPDF peak positions (Å), # of atoms in peak			
system:		1st NN	2nd NN	3rd NN	symmetry
clusters:					
NaAr	max.	4.99	---	---	C _{∞v}
	mean	5.17, 1			
NaAr ₂	max.	5.00	---	---	C _{2v}
	mean	5.12, 2			
NaAr ₃	max.	4.98	---	---	C _{3v}
	mean	5.16, 3			
NaAr ₆	max.	4.96	7.60	---	C _{2v}
	mean	5.04, 4	7.62, 2		
NaAr ₁₁	max.	4.92	7.51	8.60	C ₁
	mean	4.99, 5	7.44, 5	8.61, 1	
NaAr ₁₂	max.	4.95	7.55	8.77	C _{5v}
	mean	4.97, 6	7.56, 5	8.78, 1	
surface:	max.	4.76	6.1	7.4	---
	mean	4.76, 3½	6.0, 3¼	7.3, 9	

Table 3. Summary of calculated ensemble averaged total ground state energies, $\langle E_i(Q) \rangle_{\text{ave}}$, and the contribution from the averaged M-Rg energy, $\langle U_{\text{M-Rg}} \rangle_{\text{ave}}$, for simulations carried out at $T = 10$ K. The matrix simulation values include long range cutoff corrections of -390 cm^{-1} from the Na-Ar ground state interactions, and $-75 \text{ cm}^{-1}/\text{Ar atom}$ from the Ar-Ar interactions. All energies are rounded to the nearest 10 cm^{-1} .

system:	# of atoms in ensemble	$\langle E_i(Q) \rangle_{\text{ave}}$	$\langle U_{\text{M-Rg}} \rangle_{\text{ave}}$
clusters:			
NaAr	2	-50	-50
NaAr ₂	3	-200	-110
NaAr ₃	4	-450	-160
NaAr ₆	7	-1410	-240
NaAr ₁₁	12	-3440	-340
NaAr ₁₂	13	-3980	-390
surface site:	217	N/A	-510
matrices:			
pure fcc Ar	108	-85,060	N/A
O _h interstitial	109	-82,640	-670
O _h int. annealed	109	-82,660	-700
1-atom subst.	108	-83,870	-600
2-atom subst.	107	-82,760	-1020
3-atom subst.	106	-81,970	-1340
4-atom subst.	105	-81,340	-1750
5-atom subst.	104	-80,050	-1730
6-atom subst.	103	-79,040	-1810
13-atom subst.	96	-70,890	-1530

plus a surface Na atom, in agreement with previous findings^{74,76,77,104}. This result can be understood by considering the differences in the Na-Ar and Ar-Ar ground state pair potentials. Since the Ar-Ar potential minimum occurs at shorter separations and is deeper than the Na-Ar well, energy minimization demands the close-packed Ar structure and the exclusion of the Na atom (see also the more complete discussions based on molecular dynamics simulations in Refs. 81 and 105). Table 3 includes the ensemble averaged total ground state energy, $\langle E_i(Q) \rangle_{ave}$, and the contribution from the averaged M-Rg energy, $\langle U_{M-Rg} \rangle_{ave}$, for simulations carried out at $T = 10$ K. For these cluster systems and our choice of energy zero, the ensemble averaged ground state energy can be thought of as the "classical binding energy," averaged over the thermally accessible configurations.

At present, we could find no experimental spectral data in the literature on NaAr_n clusters for $n > 1$. Moreover, a direct comparison with results of previous structural and spectral simulations is possible only for the NaAr_6 cluster⁷⁶. Our simulations reproduce the correct equilibrium structure at $T = 10$ K: the so-called a_1 isomer in the notation of Ref. 76. Our absorption spectrum shown in Fig. 2d, and our peak positions listed in Table 1, also agree well with the simulated NaAr_6 spectrum shown in Fig. 12a of Ref. 76, from which we estimate peak positions near 16860, 17060, and 17520 cm^{-1} .

The simulated cluster absorption spectra all show two more or less resolved red components along with one broad, blue shifted component (see also Ref. 79). Since the equilibrium structures of these clusters, close packed Ar plus an excluded Na atom, introduce the Na-Ar_n axis as a strongly preferred direction, we can make an analogy to the NaAr diatomic case and attribute the absorption features to transitions to " Π -like" and " Σ -like" excited electronic states. In particular, Fig. 2 shows a progressively greater shift of the blue satellite absorption feature, which is roughly proportional to the number of Ar atoms in the first NN shell. The magnitude of the calculated shift is $\approx 150 \text{ cm}^{-1}$ per first NN Ar perturber, comparable to the difference between the $\text{NaAr}(B^2\Sigma)$ and $\text{NaAr}(X^2\Sigma)$ potentials ($\approx 250 \text{ cm}^{-1}$) at the typical first NN separation of $R \approx 5 \text{ \AA}$. We will encounter this "doublet plus singlet" absorption lineshape again in our Na/Ar surface and matrix simulations.

C. Na/Ar Surfaces

Fig. 3 shows the RPDF and simulated absorption spectrum for a Na atom trapped on a close-packed Ar {111} surface at $T = 10$ K. The plotted RPDF, and its analysis included in Table 2, indicate that at $T = 10$ K the Na atom is for the most part trapped at a three-atom hollow. However, examination of the final configuration generated in that particular simulation found the Na atom some 20 \AA from its original position, indicating that the Na

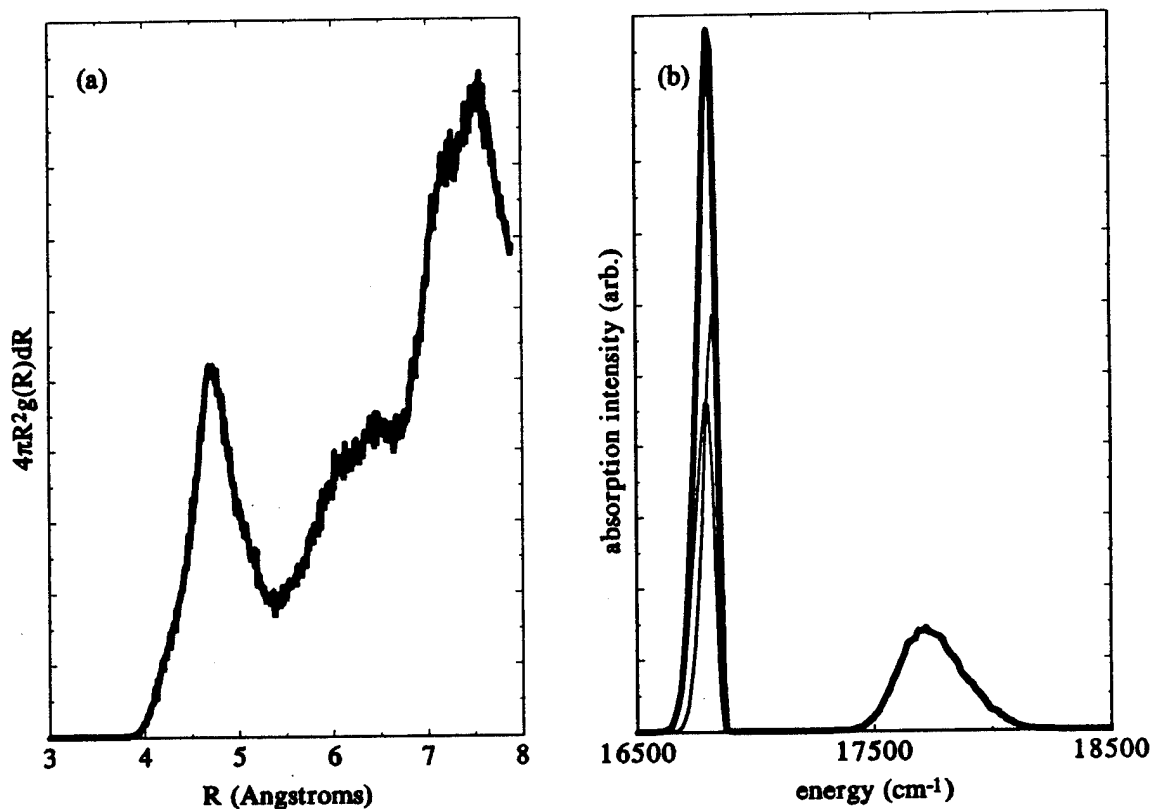


FIG. 3. Simulated RPDF and 3s→3p absorption spectrum of a Na atom on an Ar {111} surface at $T = 10$ K. Panel (a) shows the RPDF calculated for an ensemble of one Na atom and 216 Ar atoms, and employing two-dimensional periodic boundary conditions to mimic an infinite surface. The solid curve in panel (b) shows the simulated optical absorption spectrum, the thin curves show the underlying unresolved components of the red shifted doublet.

atom also regularly samples configurations connecting the various three-atom hollows. The simulated spectrum qualitatively resembles the NaAr and NaAr₃ spectra, and shows the same centroid shift as the NaAr₃ spectrum, however with a much larger splitting between the two peaks.

We also performed simulations of this system at temperatures up to $T = 50$ K. Already by $T = 30$ K most of the structure past the first peak in the RPDF was washed out, except for a broad maximum near 8 Å (almost twice the first NN separation) reminiscent of the pair distribution function for a fluid system. The Na atom remained on the exterior of the Ar surface, and we did not observe any tendency towards solvation or incorporation of the Na atom into the Ar bulk. The higher temperatures served to broaden the individual peaks in the simulated absorption spectra; for example: the FWHM of the sharp red-shifted and broad blue-shifted peaks changed from ≈ 100 cm⁻¹, and ≈ 300 cm⁻¹ at $T = 10$ K, respectively, to ≈ 150 cm⁻¹ and ≈ 600 cm⁻¹ at $T = 50$ K. In contrast, the respective peak maxima shifted only slightly, by +45 cm⁻¹ and -45 cm⁻¹.

D. Pure Solid Ar

We once again take advantage of a simple prototypical system to test our model and its computer code implementation. Table 4 includes a synopsis of the results of our simulation of the structure of pure fcc solid Ar at $T = 10$ K, which agrees with the known equilibrium structure (note however that this agreement is primarily due to our use of periodic boundary conditions and a constant volume cell). The FWHM of the second, third, and fourth NN peaks in the simulated Ar-Ar RPDF were ≈ 0.22 Å. By considering the generated positions of the non first NN Ar atoms as random independent variables, we can divide these peak widths by $\sqrt{2}$ to yield the root-mean-square displacement, $\langle u^2 \rangle^{1/2}$, for an Ar atom of ≈ 0.16 Å. This result is somewhat smaller than the value of $\langle u^2 \rangle^{1/2} \approx 0.18$ Å estimated for the quantum zero-point motion (ZPM) which dominates $\langle u^2 \rangle^{1/2}$ for solid Ar from $T = 0$ to 10 K^{106,107}. Thus, our classical Na/Ar matrix simulations should be limited to temperatures greater than $T \approx 10$ K, in order to avoid seriously underpredicting the spread of the correct quantum initial state probability distribution.

E. Na/Ar Matrices

1. Finite size effects

We checked for finite size effects, and the efficacy of our long range cutoff correction scheme, by comparing the results of simulations of a Na atom in a single atom substitutional vacancy carried out using the 6x6x6 and 8x8x8 cells. The calculated RPDFs were virtually identical, with peak positions and centroids all agreeing to within ± 0.01 Å,

Table 4. Summary of results of the Na/Ar matrix RPDF simulations at $T = 10$ K. The first entry gives the position of a peak maximum in the RPDF; the second entry gives the mean position calculated over the entire peak, and the number of Ar atoms in that peak; the third entry is the expected peak positions around the center of each site for an undistorted fcc Ar lattice. The last column lists the symmetry of the first NN shell of Ar atoms. The simulations employed the $6 \times 6 \times 6 \{100\}$ plane cell.

		<u>RPDF peak positions (Å). # of atoms in peak</u>				<u>symmetry</u>
<u>trapping site</u>		<u>1st NN</u>	<u>2nd NN</u>	<u>3rd NN</u>	<u>4th NN</u>	
pure fcc Ar	max.	3.75	5.31	6.50	7.51	---
	mean	3.75, 12	5.31, 6	6.50, 24	7.51, 12	
	ideal	3.76, 12	5.31, 6	6.51, 24	7.51, 12	
O_h interstitial	max.	3.91, 4.3sh	5.42	6.54	7.57	$\approx C_{2v}$
	mean	4.02, 13	5.37, 5	6.60, 25	7.63, 13	
	ideal	2.66, 6	4.60, 8	5.94, 24	7.97, 30	
O_h int. ann.	max.	3.96	5.35	6.59	7.60	$\approx O_h$
	mean	3.96, 12	5.26, 6	6.61, 26	7.61, 12	
	ideal	2.66, 6	4.60, 8	5.94, 24	7.97, 30	
1-atom subst.	max.	3.93	5.31	6.55	7.57	O_h
	mean	3.93, 12	5.31, 6	6.55, 24	7.57, 12	
	ideal	3.76, 12	5.31, 6	6.51, 24	7.51, 12	
2-atom subst.	max.	3.69	4.18	4.44	4.77	C_{2v}
	mean	3.70, 4	4.17, 2	4.44, 2	4.75, 4	
	ideal	3.25, 4	4.20, 4	4.97, 8	5.63, 6	
3-atom subst.	max.	3.63	3.95	4.44	4.89	C_{3v}
	mean	3.63, 1	3.96, 3	4.42, 3	4.91, 6 $\frac{1}{2}$	
	ideal	3.07, 1	3.76, 3	4.34, 3	4.85, 6	
4-atom subst.	max.	4.50	5.78	6.92	7.89	T_d
	mean	4.50, 12	5.78, 12	6.92, 16	7.87, 24	
	ideal	4.40, 12	5.79, 12	6.90, 16	7.86, 24	
5-atom subst.	max.	4.51	5.78	6.92	7.89	C_1
	mean	4.51, 11	5.78, 12	6.92, 16	7.87, 24	
6-atom subst.	max.	4.64	5.93	---	---	O_h
	mean	4.67, 8	5.94, 24	---	---	
	ideal	4.60, 8	5.94, 24	7.97, 30	---	
13-atom subst.	max.	4.69	5.25	6.4	7.45	C_{3v}
	mean	4.73, 3	5.27, 3	6.33, 19	7.39, 15	
	ideal	5.31, 6	6.51, 24	7.51, 12	---	

sh = shoulder

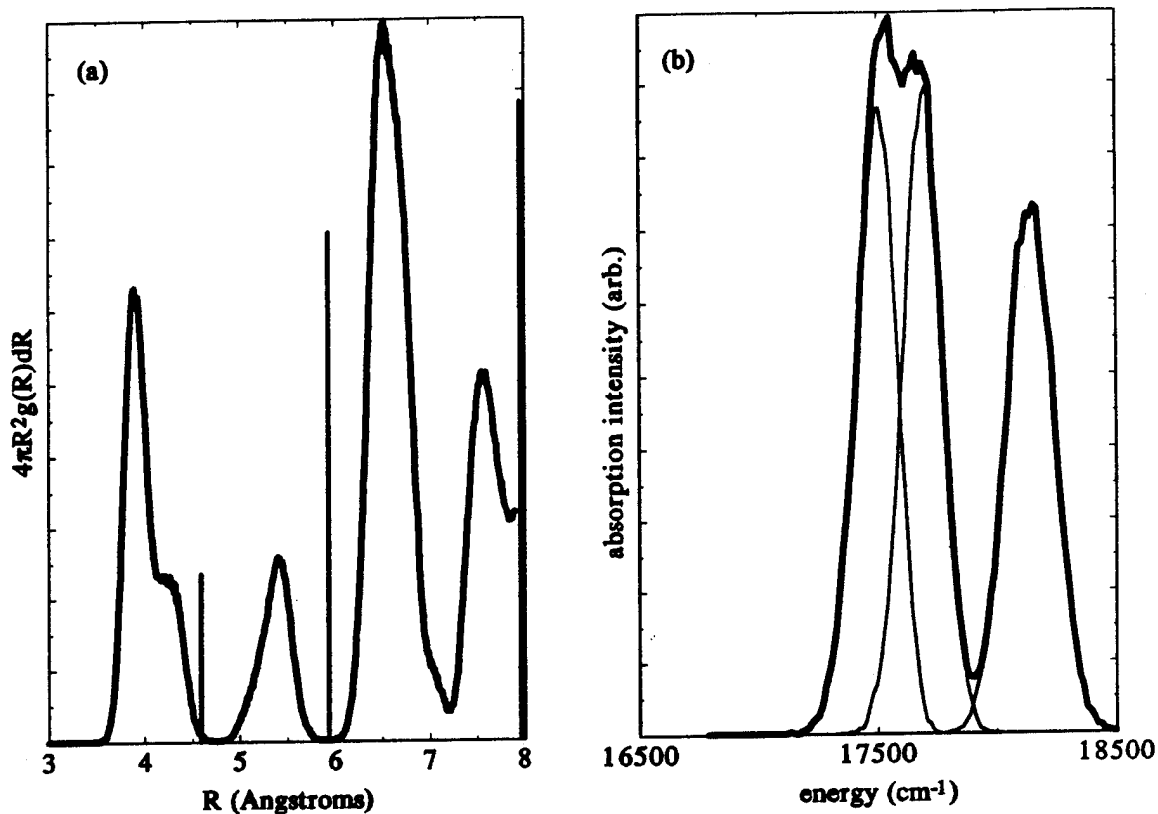


FIG. 4. Simulated RPDF and $3s \rightarrow 3p$ absorption spectrum for a Na atom in a relaxed O_h interstitial site in solid Ar at $T = 10$ K. The solid curve in panel (a) shows the RPDF calculated for an ensemble of one Na atom and 108 Ar atoms in a volume normally occupied by 108 Ar atoms in solid Ar. The vertical bars indicate the positions of the second through fourth NN shells around an unrelaxed O_h interstitial site. The solid curve in panel (b) shows the simulated optical absorption spectrum, the thin curves show the individual underlying components.

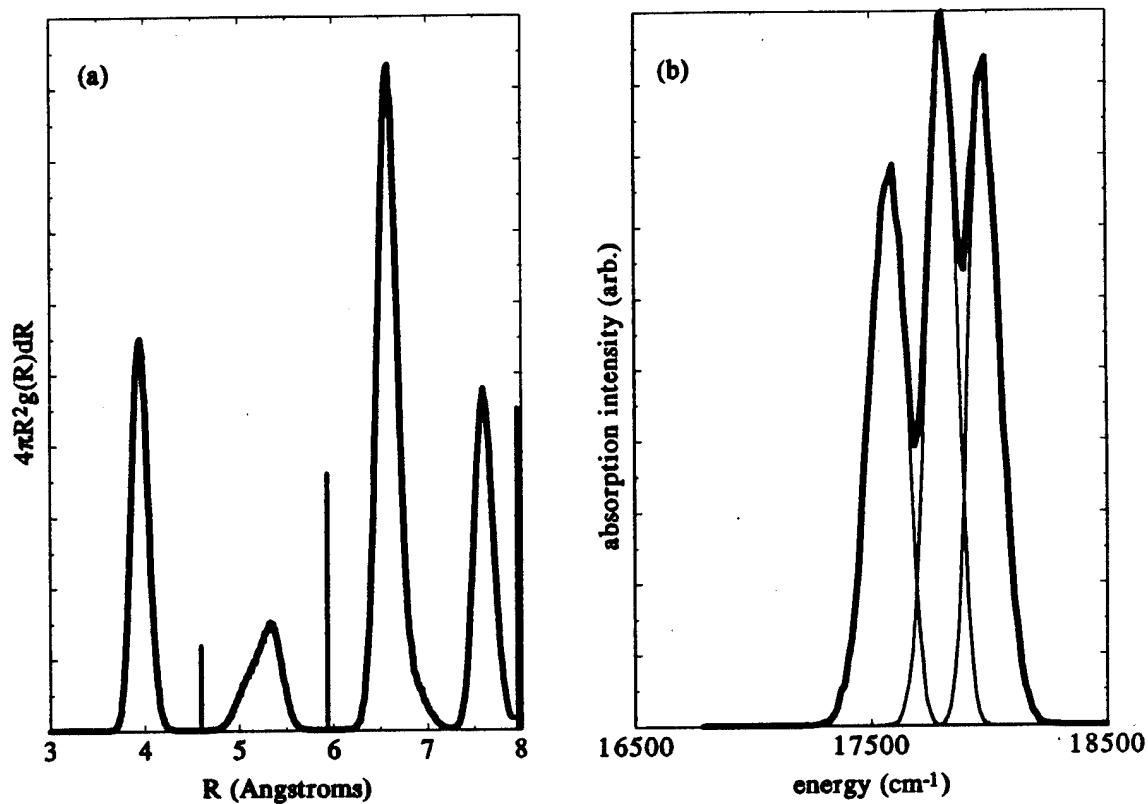


FIG. 5. Simulated RPDF and $3s \rightarrow 3p$ absorption spectrum for a Na atom in a relaxed O_h interstitial site in solid Ar at $T = 10$ K, after "annealing" to $T = 50$ K. The solid curve in panel (a) shows the RPDF calculated for an ensemble of one Na atom and 108 Ar atoms in a volume normally occupied by 108 Ar atoms in solid Ar. The vertical bars indicate the positions of the second through fourth NN shells around an unrelaxed O_h interstitial site. The solid curve in panel (b) shows the simulated optical absorption spectrum, the thin curves show the individual underlying components.

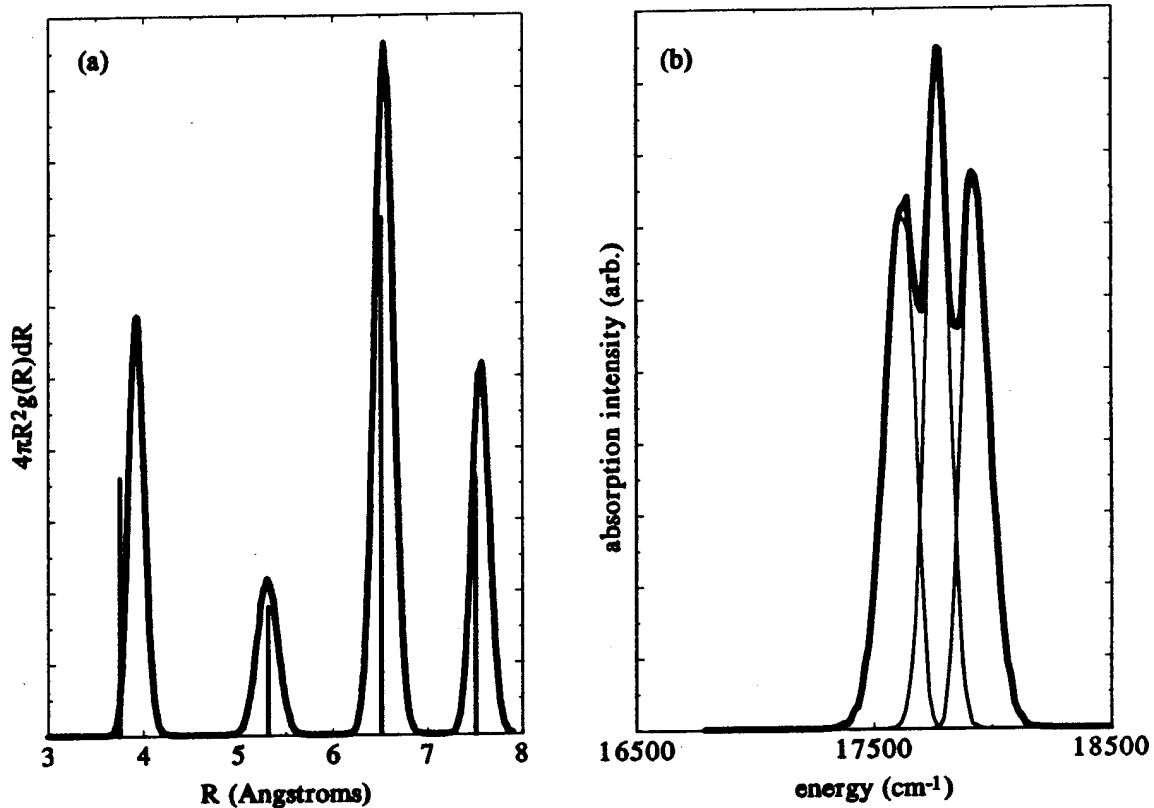


FIG. 6. Simulated RPDF and $3s \rightarrow 3p$ absorption spectrum for a Na atom in a relaxed one-atom substitutional site in solid Ar at $T = 10$ K. The solid curve in panel (a) shows the RPDF calculated for an ensemble of one Na atom and 107 Ar atoms in a volume normally occupied by 108 Ar atoms in solid Ar. The vertical bars indicate the positions of the first four NN shells around an unrelaxed single substitutional site. The solid curve in panel (b) shows the simulated optical absorption spectrum, the thin curves show the individual underlying components.

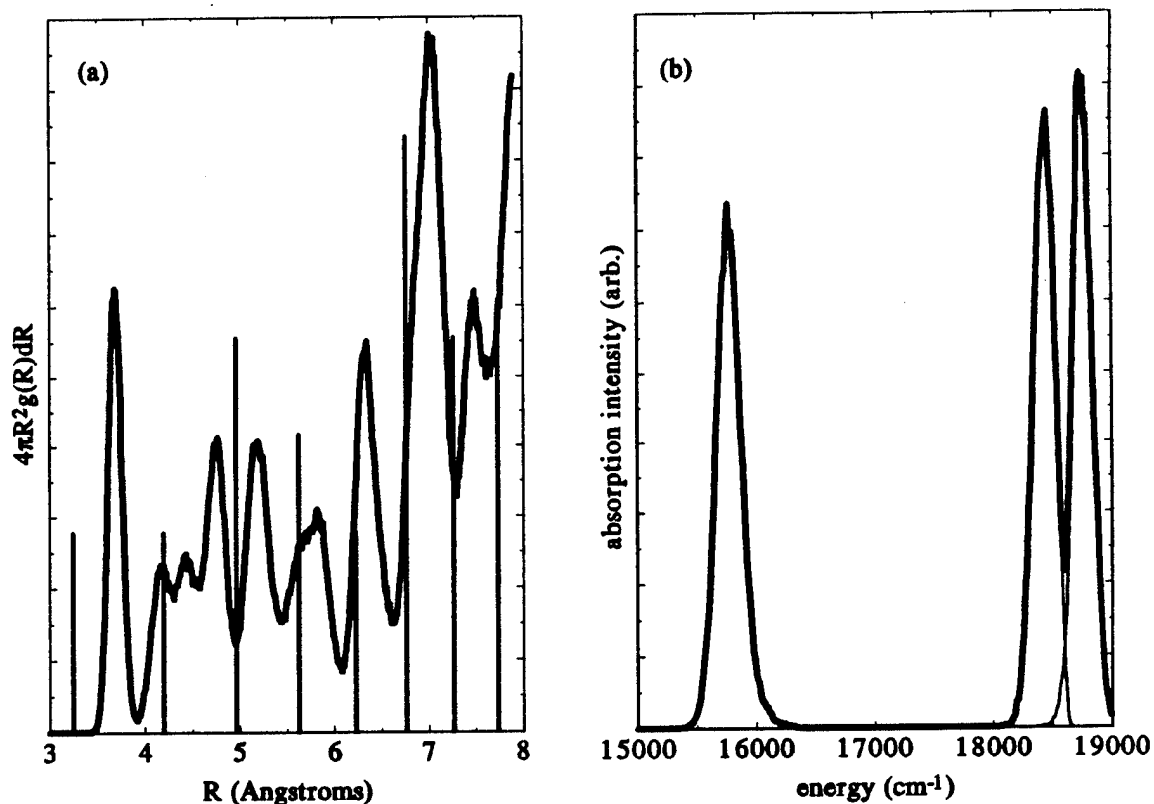


FIG. 7. Simulated RPDF and $3s \rightarrow 3p$ absorption spectrum for a Na atom in a relaxed two-atom vacancy in solid Ar at $T = 10$ K. The solid curve in panel (a) shows the RPDF calculated for an ensemble of one Na atom and 106 Ar atoms in a volume normally occupied by 108 Ar atoms in solid Ar. The vertical bars indicate the positions of the first eight NN shells around the center of an unrelaxed two-atom substitutional site. The solid curve in panel (b) shows the simulated optical absorption spectrum, the thin curves show the individual underlying components.

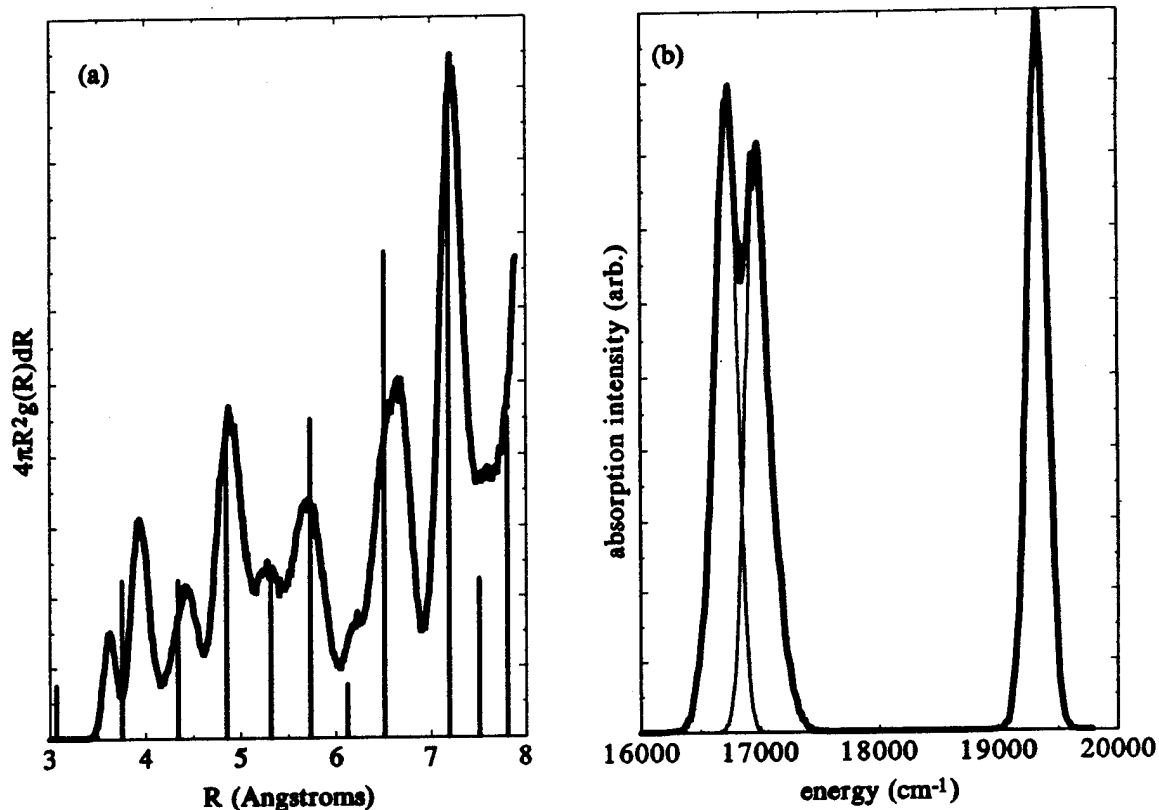


FIG. 8. Simulated RPDF and 3s→3p absorption spectrum for a Na atom in a relaxed three-atom vacancy in solid Ar at $T = 10$ K. The solid curve in panel (a) shows the RPDF calculated for an ensemble of one Na atom and 105 Ar atoms in a volume normally occupied by 108 Ar atoms in solid Ar. The vertical bars indicate the positions of the first eleven NN shells around the center of an unrelaxed three-atom substitutional site. The solid curve in panel (b) shows the simulated optical absorption spectrum, the thin curves show the individual underlying components.

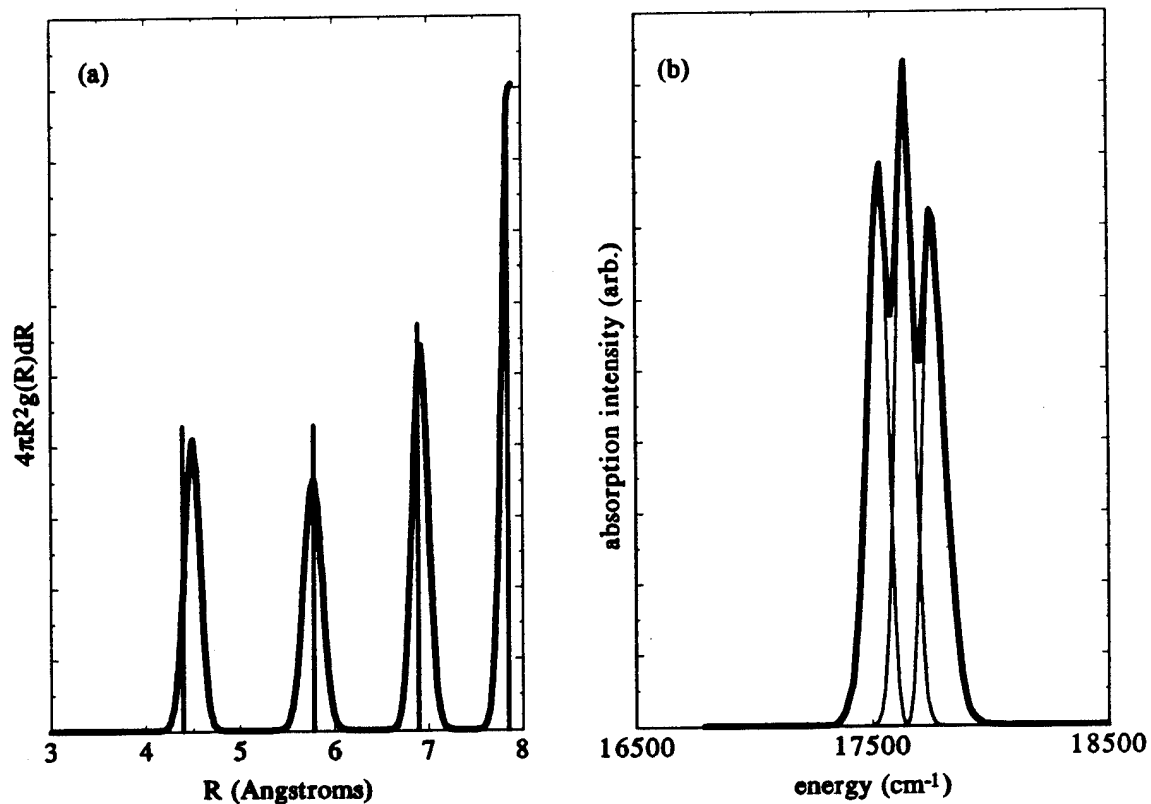


FIG. 9. Simulated RPDF and $3s \rightarrow 3p$ absorption spectrum for a Na atom in a relaxed four-atom vacancy in solid Ar at $T = 10$ K. The solid curve in panel (a) shows the RPDF calculated for an ensemble of one Na atom and 104 Ar atoms in a volume normally occupied by 108 Ar atoms in solid Ar. The vertical bars indicate the positions of the first four NN shells around the center of an unrelaxed tetrahedral four-atom vacancy. The solid curve in panel (b) shows the simulated optical absorption spectrum, the thin curves show the individual underlying components.

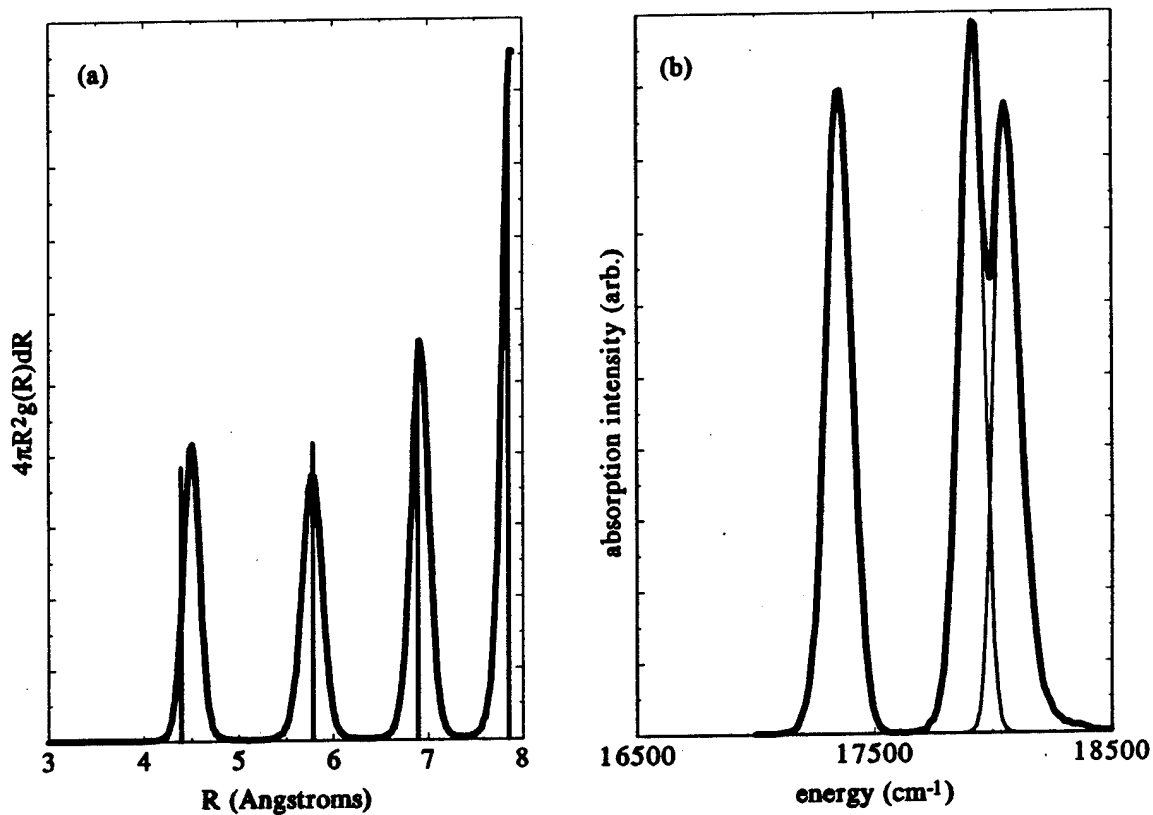


FIG. 10. Simulated RPDF and $3s \rightarrow 3p$ absorption spectrum for a Na atom in a relaxed five-atom vacancy in solid Ar at $T = 10$ K. The solid curve in panel (a) shows the RPDF calculated for an ensemble of one Na atom and 103 Ar atoms in a volume normally occupied by 108 Ar atoms in solid Ar. The vertical bars indicate the positions of the first four NN shells around the center of an unrelaxed *tetrahedral four-atom vacancy*. The solid curve in panel (b) shows the simulated optical absorption spectrum, the thin curves show the individual underlying components.

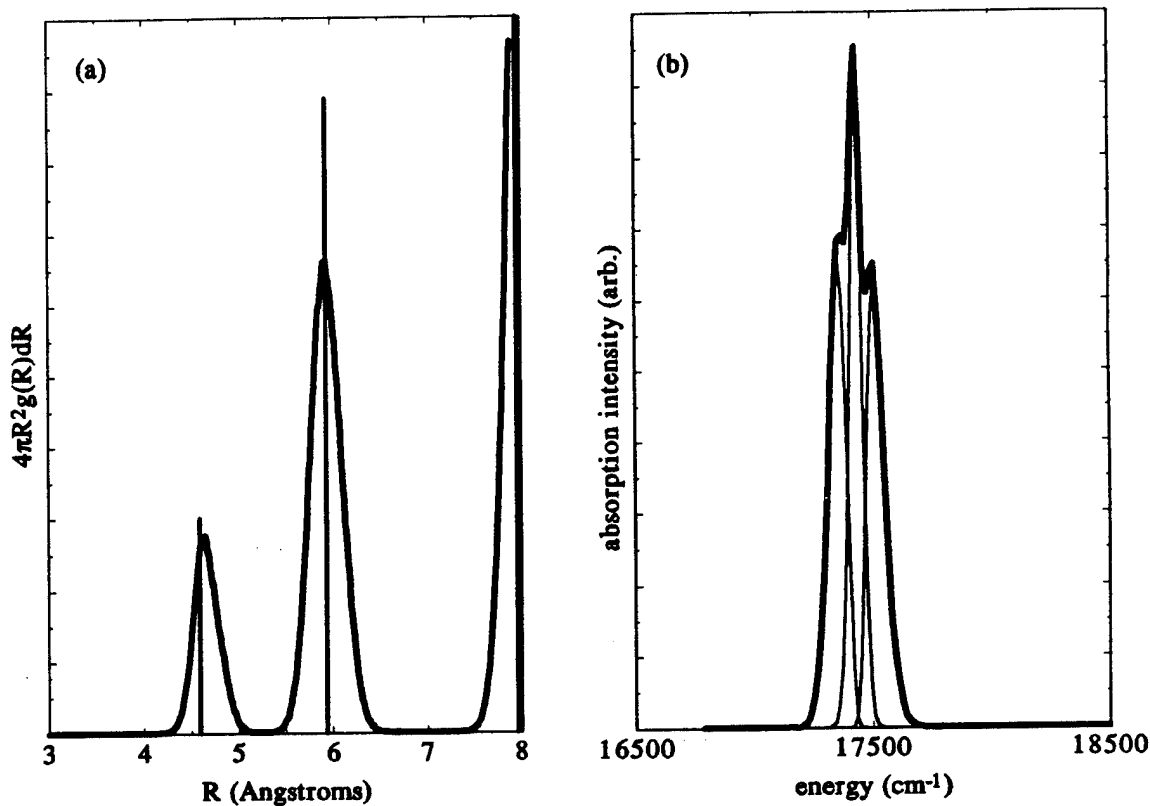


FIG. 11. Simulated RPDF and $3s \rightarrow 3p$ absorption spectrum for a Na atom in a relaxed six-atom vacancy in solid Ar at $T = 10$ K. The solid curve in panel (a) shows the RPDF calculated for an ensemble of one Na atom and 102 Ar atoms in a volume normally occupied by 108 Ar atoms in solid Ar. The vertical bars indicate the positions of the first three NN shells around the center of an unrelaxed octahedral six-atom vacancy. The solid curve in panel (b) shows the simulated optical absorption spectrum, the thin curves show the individual underlying components.

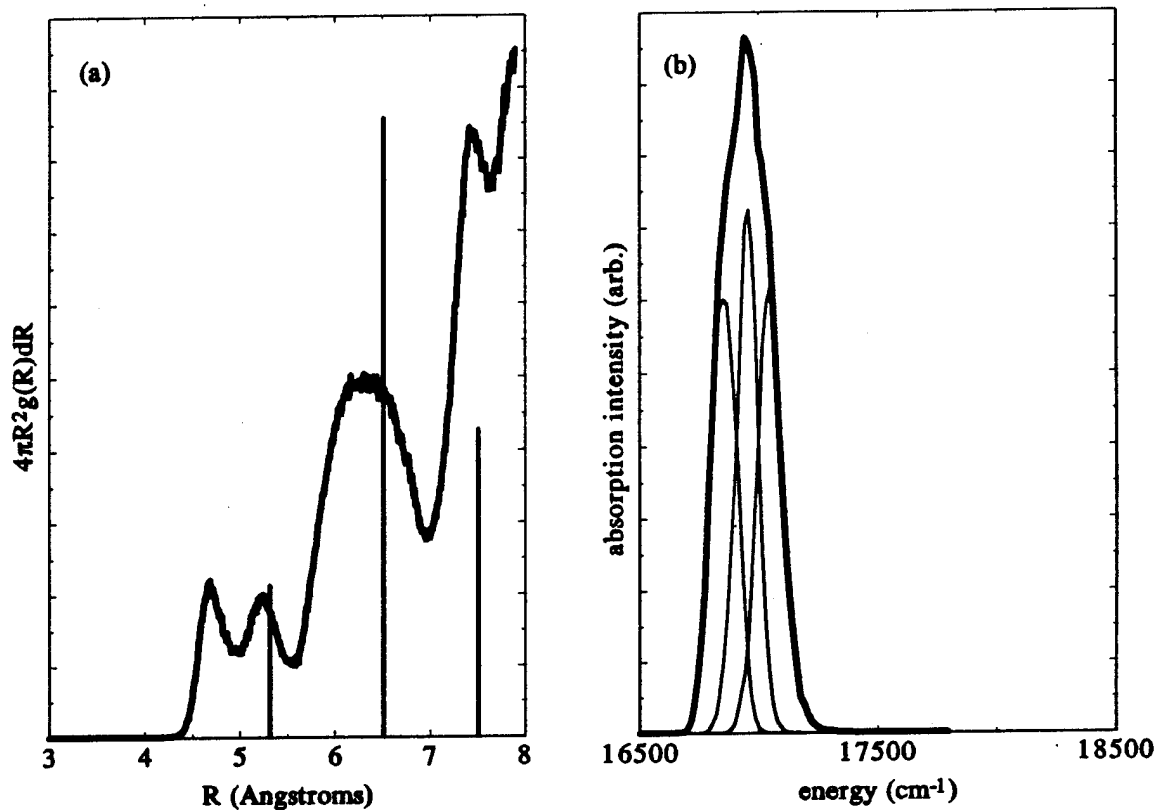


FIG. 12. Simulated RPDF and $3s \rightarrow 3p$ absorption spectrum for a Na atom in a relaxed thirteen-atom vacancy in solid Ar at $T = 10$ K. The solid curve in panel (a) shows the RPDF calculated for an ensemble of one Na atom and 95 Ar atoms in a volume normally occupied by 108 Ar atoms in solid Ar. The vertical bars indicate the positions of the first three NN shells around the center of an unrelaxed octahedral thirteen-atom vacancy. The solid curve in panel (b) shows the simulated optical absorption spectrum, the thin curves show the individual underlying components.

from which we conclude that the use of the 6x6x6 108 atom cell is sufficient to obtain the correct, size converged trapping site structures for this system, and for the multi-substitutional trapping sites. Likewise the *splittings* between the peaks in the calculated optical absorption spectra agreed to within the 15 cm⁻¹ spectral bin size. However, neglecting long range corrections to the spectral shifts lead to a strong dependence of the absolute position of the *centroid* of the absorption band on the size of the ensemble. For example, the uncorrected gas-to-matrix centroid shift for the 6x6x6 cell was +1010 cm⁻¹, as compared to +845 cm⁻¹ for the 8x8x8 cell. The long range corrections appropriate for these two cases are -210 cm⁻¹, and -50 cm⁻¹, respectively, resulting in good agreement between the final, corrected centroid shifts of +800 cm⁻¹ and +795 cm⁻¹, respectively. All of the calculated spectral shifts and total energies from the Na/Ar matrix simulations reported in the tables include the appropriate long range corrections.

2. Simulations at $T = 10$ K

Figs. 4 through 12 show the results of our simulations of the relaxed structures and optical absorption spectra of Na/Ar matrices at $T = 10$ K, for initial geometries based on O_h interstitial, annealed O_h interstitial, and one, two, three, four, five, six, and thirteen-atom substitutional vacancies in fcc Ar, in that order. The spectral data are summarized in table I, the calculated mean ground state energies in Table 3, and the RPDFs in Table 4.

The relaxed trapping site structure simulated at $T = 10$ K for a Na atom initially placed in an O_h interstitial site (Fig. 4a) appears to be a "crowded" version of the relaxed one-atom substitutional site (Fig. 6a), with thirteen instead of twelve first NN Ar atoms around the Na atom. Comparison of the positions of the peaks in the Na-Ar RPDF in Fig. 4a with the vertical bars representing the expected peaks around an O_h interstitial site indicates the gross rearrangement resulting from relaxation. The extra first NN Ar atom reduces the symmetry of the equilibrium positions of the Ar atoms in the first NN shell from O_h to roughly C_{2v} . This "static" distortion is responsible for the "doublet plus singlet" absorption lineshape.

We tested for the possibility of other relaxed trapping site structures based on the O_h interstitial site by running the same simulations at temperatures up to $T = 50$ K, and then quenching back to $T = 10$ K. We loosely refer to this procedure as "annealing" the ensemble, and to the resulting new trapping site structure as the "annealed," relaxed O_h interstitial site. Fig. 5 shows the RPDF and absorption spectrum for this trapping structure in which extra Ar atoms appear in the third NN shell. The local structure around the Na atom is very similar to that around the relaxed one-atom substitutional site, and the

absorption spectrum shows only a minor asymmetry in its triplet pattern. As Table 3 shows, the two O_h interstitial based trapping structures differ in total energy by only $\approx 20 \text{ cm}^{-1}$, making an absolute assignment of the global minimum geometry problematical. We attempted, quixotically, to produce the annealed, relaxed structure directly at $T = 10 \text{ K}$ by initially introducing the Na atom into a one-atom substitutional site and adding an extra Ar atom to the third NN shell. In all these cases the ensemble reverted back to the locally crowded structure depicted in Fig. 4a.

The simulated spectrum for a Na atom in a relaxed single substitutional vacancy at $T = 10 \text{ K}$ presented in Fig. 6b shows the classic triplet absorption pattern ubiquitous to Na/Rg matrix spectra. Fig. 6a and Table 4 show that the ensemble required only minor radial relaxation of the Ar atoms surrounding the central Na atom to reach equilibrium. This result is somewhat surprising to us, since an estimate of the relative "volumes" of the Na and Ar atoms based on Eq. 1 from Ref. 23 and the Na-Ar and Ar-Ar pair potentials indicates that the removal of roughly two Ar atoms is required to accommodate a Na atom. However, these simulations suggest that the Ar lattice is capable of supporting a Na atom in even tighter trapping sites.

Introducing a Na atom into a two-atom vacancy at $T = 10 \text{ K}$ once again results in a relaxed trapping site structure with an equilibrium symmetry low enough to split the excited Na^* states into a doublet plus singlet pattern. However, in this case the doublet to singlet splitting shown in Fig. 7b is nearly 3000 cm^{-1} . Fig. 7a shows the RPDF for this site which indicates an outward relaxation by the four first NN Ar atoms of $\approx 0.5 \text{ \AA}$ from their initial positions, and the splitting of the second NN peak into two distinct features. The third and fourth NN shells appear to actually contract towards the central Na atom. This relaxation results in a local equilibrium trapping structure of approximately C_{2v} symmetry.

Fig. 8 shows the RPDF and spectrum for a Na atom in a three-atom substitutional vacancy at $T = 10 \text{ K}$. The equilibrium local trapping environment symmetry is C_{3v} , with one Ar atom on the C_3 axis pushed very close to the Na atom. As for the two-atom vacancy case, the absorption spectrum shows a strongly split doublet plus singlet pattern. This trapping site results in the largest shift of a spectral feature observed in this study: the singlet component is shifted about $+2400 \text{ cm}^{-1}$ from the free Na atom transition energy.

The four-atom substitutional vacancy readily accepts a Na atom with only $\approx 0.1 \text{ \AA}$ radial distortion of the first NN shell Ar atoms required for equilibration at $T = 10 \text{ K}$. This expansion is due more to the absence of the long range attraction usually contributed by the four removed Ar atoms than to repulsive interactions with the substituted Na atom. The resulting RPDF and absorption spectrum are shown in Fig. 9. The first NN Ar atom shell

has T_d symmetry, and the corresponding absorption spectrum shows a symmetrical triplet feature similar to that for the O_h one-atom vacancy.

The five-atom substitutional site also readily accommodates a Na atom at $T = 10$ K. The RPDF shown in Fig. 10a indicates a structure very similar to the four-atom T_d vacancy, however with only eleven Ar atoms in the first NN shell. The missing atom reduces the local trapping site equilibrium symmetry to C_1 and results in a doublet plus singlet absorption feature.

Fig. 11 shows the results of the simulation of a Na atom in a six-atom vacancy at $T = 10$ K. The Ar trapping cage retains its O_h symmetry. At this low temperature, the thermal trapping site geometry fluctuations are barely able to split the absorption lineshape into the triplet pattern.

Fig. 12 shows the simulated RPDF and absorption spectrum for a Na atom in a spacious thirteen-atom vacancy at $T = 10$ K. This vacancy was created by removing an Ar atom and its twelve first NN Ar atoms from the fcc lattice. Since the distance from the center of this site to the nuclei of the first NN Ar atoms (≈ 5.3 Å) is larger than the equilibrium separation of the Na-Ar ground state pair potential (≈ 5.0 Å), the Na atom will experience a very flat potential surface near the cage center, allowing it to readily sample off-center positions. However, this form of "long-range" asymmetry is apparently ineffective in splitting the degeneracy of the excited Na^* atom, and the absorption spectrum in Fig. 12b shows only a single broad peak, almost unshifted from the gas phase transition energy.

Examination of the absorption band centroid shifts listed in Table 1 confirms the expected trend towards increased gas-to-matrix blue shifts for smaller volume trapping sites. Furthermore, the magnitude of the calculated centroid spectral shifts can be accurately estimated from Eq. 22 by substituting for each $\langle R_k \rangle_{ave}$ the position of the centroid of the RPDF peak containing that particular Ar atom. For example, for the single substitutionally trapped Na atom, including the 54 Ar atoms comprising the first through fourth NN shells into Eq. 25, and the -210 cm^{-1} long range cutoff correction, yields an estimated band centroid shift of $+810$ cm^{-1} , very close to the calculated $+800$ cm^{-1} listed in Table 1.

3. Temperature Effects

In order to test the effects of larger fluctuations from the equilibrium trapping site structures on the absorption spectra, we also performed a few simulations at temperatures up to $T = 50$ K. Fig. 13 shows the results for an initially interstitially trapped Na atom; at the higher temperatures the absorption feature changes from the doublet plus singlet lineshape to a more symmetric triplet pattern. In fact, the $T = 50$ K interstitial absorption spectrum

NaAr108

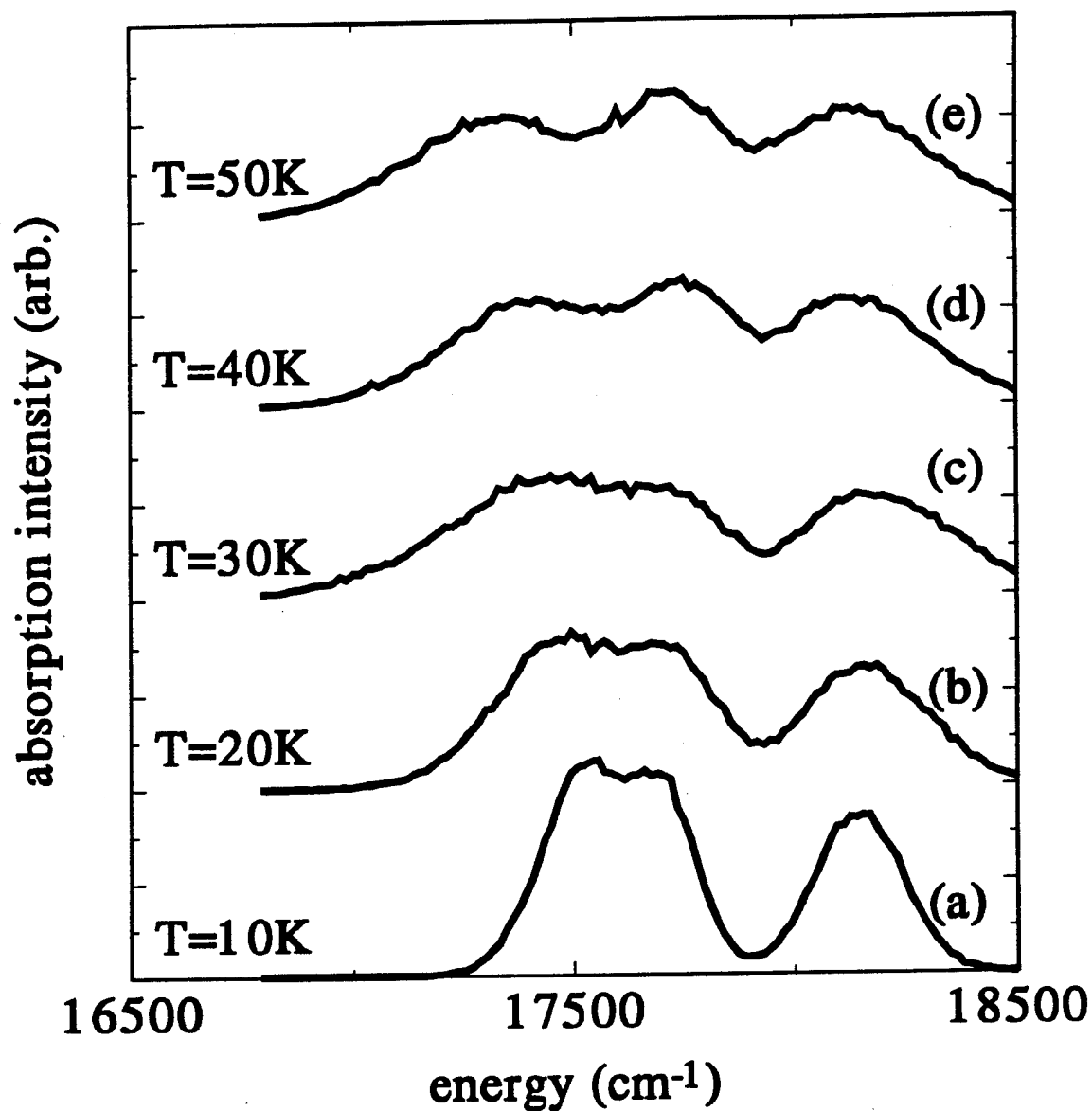


FIG. 13. Temperature dependence of the simulated $3s \rightarrow 3p$ absorption spectrum for a Na atom in a relaxed O_h interstitial site in solid Ar. Traces (a) through (e) show the spectra calculated for $T = 10$ K to 50 K, in 10 K increments. The spectrum changes from a doublet plus triplet pattern to the classic triplet pattern at the higher temperatures.

strongly resembles the spectrum calculated for a single substitutionally trapped Na atom at the same temperature, as can be seen from a comparison with Fig. 14e and the peak positions listed in Table 5. A comparison of the RPDFs for the two systems at $T = 50$ K (not shown) reveals them to be virtually identical, except for extra Ar atoms in the third NN shell in the interstitial case. As was discussed above, lowering the simulated temperature yielded the relaxed, annealed trapping structure depicted in Fig. 5. The various spectra for the single substitutional system plotted in Fig. 14 show a general increase in both the separations between the components of the triplet, and in their individual linewidths, with increasing temperature. Fig. 15 shows the same behavior for the components of the blue shifted doublet in the absorption spectra of a Na atom in a two-atom vacancy. However, for this trapping site the higher temperatures do not convert the spectrum into the classic triplet lineshape.

VI. DISCUSSION

A. Contributions of the Present Model

As promising as some of our results appear at first glance, we must conclude that our model fails to *quantitatively* predict or explain the experimental absorption spectra of Na/Ar matrices. Consideration of the experimental data summarized in Table 6 shows that we do not reproduce the exact magnitudes of either the absorption peak splittings, nor of the gas-to-matrix shifts of the centroids, for any given triplet feature. Nonetheless, our model does yield good *qualitative* agreement with many aspects of the experimental data. These partial successes encourage us to attempt to extract from our efforts at least a few generally or specifically applicable conclusions.

First, our simulations succeeded in producing several, plausible, candidate trapping sites for the Na/Ar matrix system, in agreement with the multiple trapping sites observed experimentally. We confirmed that true interstitial sites in the Ar solid cannot support an intruding Na atom without undergoing major rearrangement upon relaxation. Thus, the notion of a characteristic minimum trapping site volume²³ for a given van der Waals guest/host system appears vindicated, even if our back of the envelope method for predicting that minimum volume (embodied by Eq. 1 from Ref. 23) failed.

We are tempted to try to use the calculated average total ground state energies listed in Table 3 to choose a most stable, and hence "preferred," Na atom trapping site structure. Such an approach would select the close packed Ar solid plus an excluded Na atom as the preferred structure, over even the relaxed Na/Ar trapping site originating as a one-atom vacancy. However, we remind the reader that the experimental M/Rg matrix systems are in practice produced by depositions at a surface not at true thermodynamic equilibrium, and

NaAr107

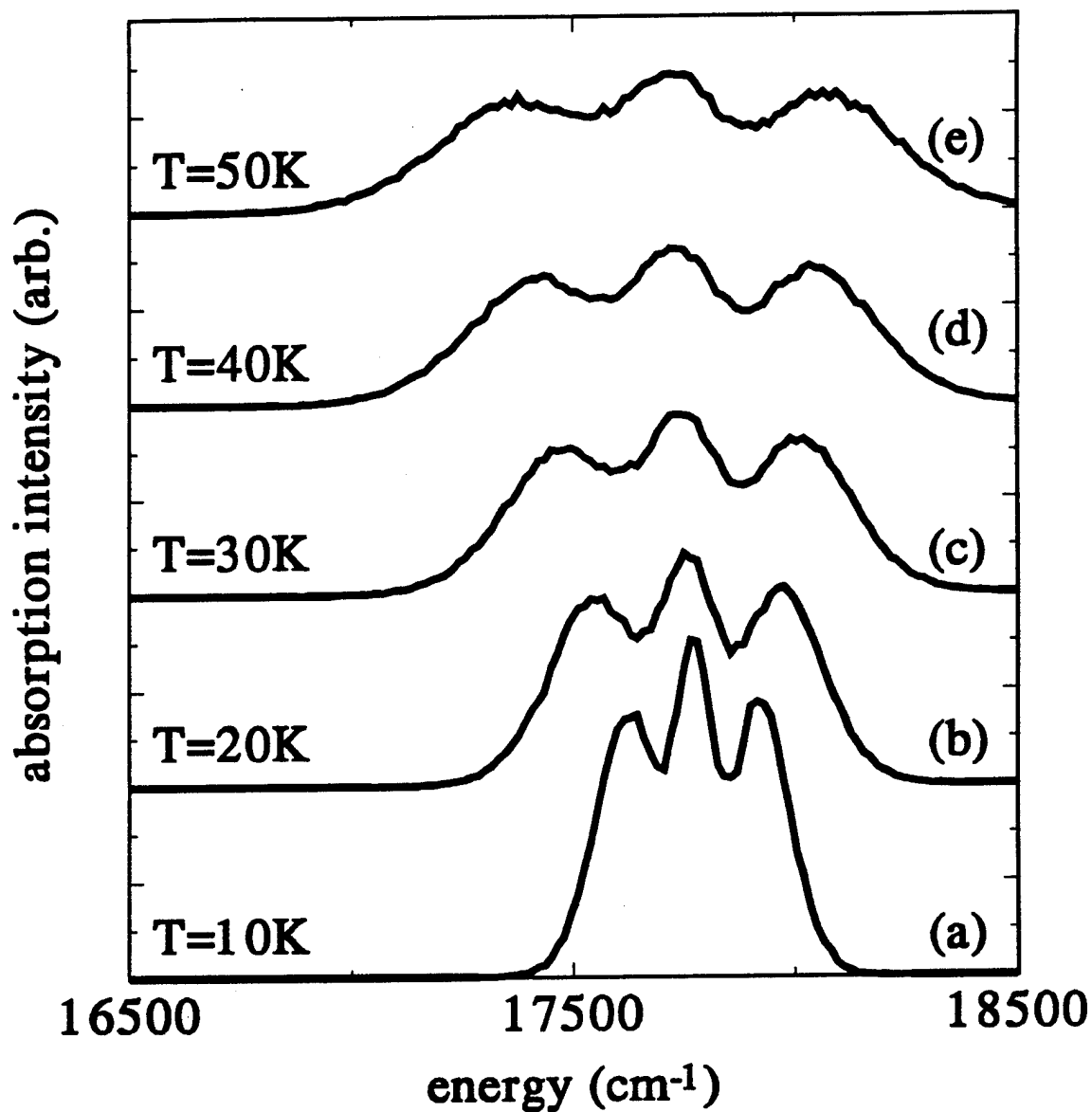


FIG. 14. Temperature dependence of the simulated $3s \rightarrow 3p$ absorption spectrum for a Na atom in a relaxed one-atom substitutional site in solid Ar. Traces (a) through (e) show the spectra calculated for $T = 10 \text{ K}$ to 50 K , in 10 K increments. The spectrum retains its classic triplet lineshape at all temperatures.

NaAr106

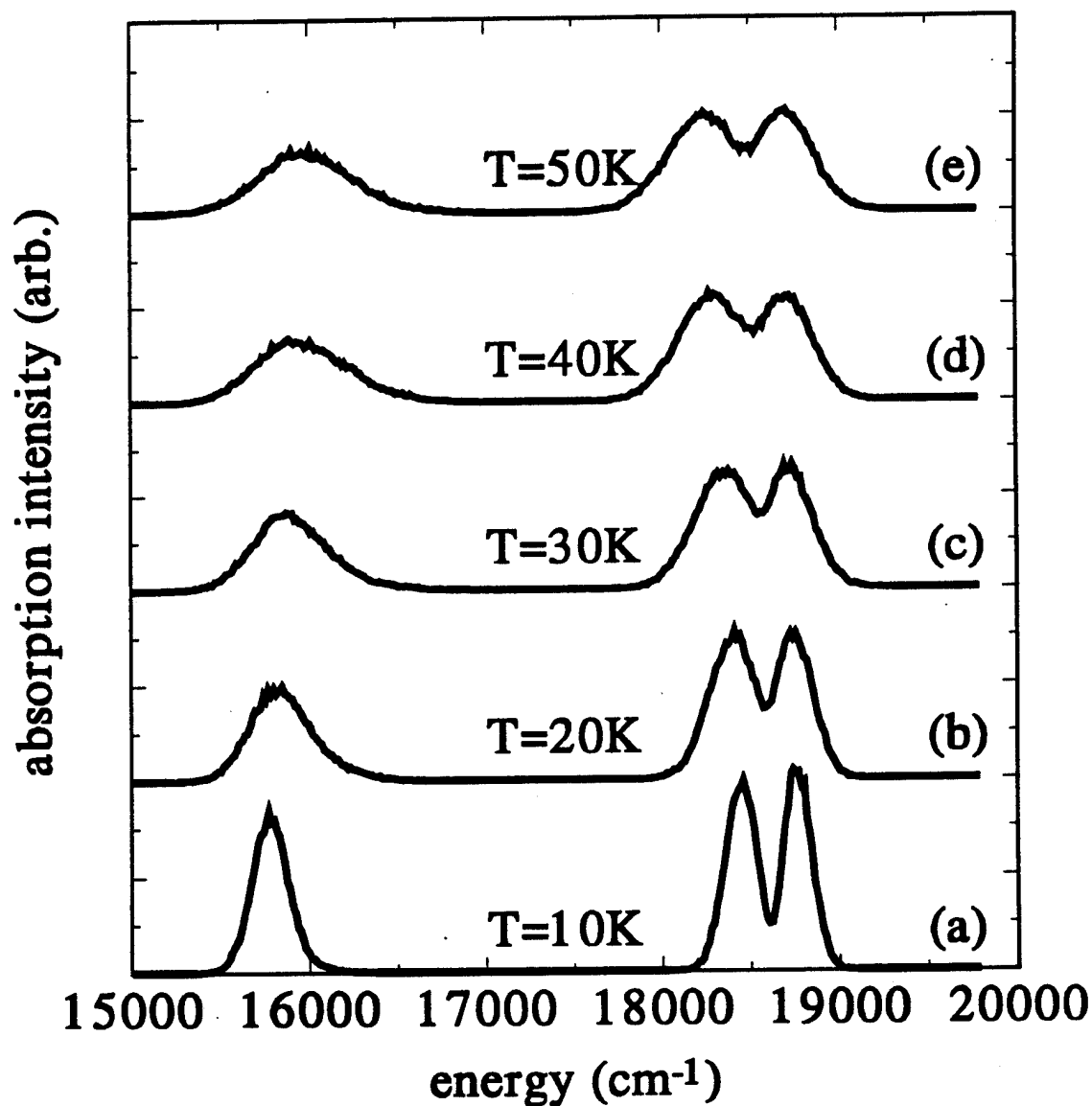


FIG. 15. Temperature dependence of the simulated $3s \rightarrow 3p$ absorption spectrum for a Na atom in a relaxed two-atom substitutional site in solid Ar. Traces (a) through (e) show the spectra calculated for $T = 10$ K to 50 K, in 10 K increments. The spectrum retains its doublet plus singlet lineshape at all temperatures.

Table 5. Summary of temperature dependence of the optical absorption peaks calculated in this study. The simulations of the O_h interstitial site at 10, 20, and 30 K represent the unannealed trapping site structure (see text). These simulations employed the $6 \times 6 \times 6 \{100\}$ plane cell and the values in this table include a long range cutoff correction of -210 cm^{-1} . Peak positions are rounded to the nearest 15 cm^{-1} , and shifts from the free Na atom $3s(^2S) \rightarrow 3p(^2P)$ transitions centered around 16968 cm^{-1} are rounded to the nearest 5 cm^{-1} .

<u>system</u>	<u>absorption peak energies (cm^{-1})</u>	<u>peak shifts from free Na atom (cm^{-1})</u>	<u>centroid shift (cm^{-1})</u>
O_h interstitial			
T = 10 K	17540, 17675, 18155	+570, +710, +1185	+805
T = 20 K	17495, 17690, 18170	+525, +720, +1200	+790
T = 30 K	17450, 17675, 18185	+480, +710, +1215	+750
T = 40 K	17405, 17750, 18140	+435, +780, +1170	+770
T = 50 K	17345, 17720, 18125	+375, +750, +1155	+740
1-atom subst.			
T = 10 K	17630, 17765, 17930	+660, +795, +960	+800
T = 20 K	17540, 17765, 17975	+570, +795, +1005	+785
T = 30 K	17480, 17750, 18020	+510, +780, +1050	+770
T = 40 K	17420, 17735, 18050	+450, +765, +1080	+755
T = 50 K	17375, 17735, 18080	+405, +765, +1110	+740
2-atom subst.			
T = 10 K	15770, 18455, 18770	-1200, +1485, +1800	+690
T = 20 K	15815, 18410, 18740	-1155, +1440, +1770	+685
T = 30 K	15875, 18365, 18740	-1095, +1395, +1770	+680
T = 40 K	15935, 18290, 18725	-1035, +1320, +1755	+670
T = 50 K	15965, 18245, 18710	-1005, +1275, +1740	+665

Table 6. Summary of experimentally observed optical absorptions of Na/Ar matrices. Peak positions given in cm^{-1} ; data from Reference 14. Peak shifts are relative to the gas phase Na atom $3s(^2S) \rightarrow 3p(^2P)$ transitions centered around 16968 cm^{-1} .

<u>Feature nomenclature</u>	<u>As deposited samples</u>		<u>Annealed samples</u>	
	<u>peaks</u>	<u>shifts</u>	<u>peaks</u>	<u>shifts</u>
red triplet	16830	-140	N/A	
	17080	+110		
	17440	+470		
blue triplet	18050	+1080	18100	+1130
	18360	+1390	18390	+1420
	18670	+1700	18680	+1710
violet triplet	19130	+2160	19120	+2150
	19510	+2540	19570	+2600
	19820	+2850	19840	+2870
"460 nm" absorption	21930	+4960	21930	+4960

furthermore can exhibit multiple M atom trapping sites within the same sample. Thus, even correct free-energy calculations utilizing more general ensembles than we employed cannot by themselves unambiguously designate a "preferred" trapping site for the matrix deposition process.

Our calculated energetics do, however, suggest a further refinement of the microscopic trapping site formation dynamics model developed in Refs. 13, 14, and 23. Our discussions of the trapping site generation mechanisms have so far focused on the relative thermodynamic stabilities, and hence total energies, of the candidate trapping sites. For example, we have explained the absence of the novel Na/Ar violet triplet absorption in matrices produced using slow Knudsen oven generated Na atoms as due to the inability of these atoms to access the "high energy" site responsible for the violet triplet¹⁴. However, the results in Table 3 show only small differences in the calculated total energies for the various candidate tight sites. This suggests that for the Na/Ar system the repulsive forces which arise from the small Na-Ar separations may be the determining factor in trapping site formation, rather than the total Na/Ar system energy. Thus, for other than thermodynamically equilibrated bulk Na/Ar systems, the localized stresses associated with these repulsive interactions may dynamically favor the formation of larger volume trapping sites. We hope to resolve more of the details of this model in the future via use of the molecular dynamics simulation method.

We note a surprisingly clean separation of the effects on the absorption spectra of "static" vs. "dynamic" distortions of the Na atom trapping environment. More precisely: *(1) trapping sites in which the equilibrium positions of the atoms form a structure belonging to a high symmetry point group (i.e., O_h or T_d) yield the classic triplet absorption pattern.* In these cases the splitting of the degeneracy of the excited Na* atom 2P state can only be due to fluctuations away from the equilibrium trapping site structure. This conclusion is further supported by the results of simulations of these highly symmetrical sites at higher temperatures, which show an increase in the peak splittings with temperature. Conversely: *(2) trapping environments with equilibrium structures of lower symmetry, in which a strongly preferred direction exists (i.e., C or D point groups), exhibit a well-separated doublet plus singlet absorption pattern.* For these sites the static axial asymmetry dominates the doublet to singlet splitting, while geometry fluctuations determine the splitting within the doublet feature itself. In the specific case of the Na atom trapped in the two-atom vacancy, we also showed that this axial asymmetry and the associated doublet plus singlet pattern persists even to $T = 50$ K. Alternatively: *(3) trapping sites with only minor deviations from a highly symmetrical structure (e.g., the initially interstitial site) can yield the doublet plus singlet pattern at low temperatures, and a symmetrical triplet pattern at higher temperatures.* The

increased magnitude of the geometry fluctuations at higher temperature apparently overwhelms the original axial asymmetry of these sites. Such intermediate cases provide for a direct comparison of the relative importance of static and dynamic distortions in determining the absorption lineshape. Finally, we also note that "tighter" trapping structures, *i.e.*, those corresponding to smaller vacancies or to lower temperatures for a given trapping site, typically give larger blue shifts of the centroid of the absorption band than do "looser" structures.

We should point out here that our omission of any simulations of amorphous matrix or liquid structures further limits the generality of some of our conclusions. If one considers each different nuclear configuration, Q , as a distinct "isomer" of the Na/Ar system, then our calculated absorption lineshapes can be thought of as inhomogeneously broadened spectra in the sense that they are calculated as an average over the multitude of isomers. Since our MC method in principle does not include any dynamical effects, we cannot distinguish between an ensemble average taken over a superposition of static amorphous sites vs. an average over dynamically distorted crystalline sites. Thus, our results do not preclude the possibility that simulations of amorphous or liquid Na/Ar systems may also yield well defined triplet absorption features.

B. Comparison with Experiments and Previous Models

Even though our results do not allow us to make any definite assignments between a given triplet absorption feature and a proposed trapping site structure, we can now speculate on the nature of the trapping sites from a better informed perspective. We associate the observed red, blue, and violet triplet absorptions with Na atoms trapped at sites lacking a single strongly preferred direction; perhaps even with sites possessing equilibrium structures of high symmetry. This assignment further constrains our recent adoption¹⁴ of a previously proposed model⁴² of the red triplet site structure as "Na atoms trapped at or very near to internal surface defects in the matrix." Our present view is that Na atom trapped even on atomically rough Rg surfaces would exhibit a doublet plus singlet absorption pattern, not the observed symmetrical triplet feature. We thus refine our model of the red triplet absorption to include only Na atoms trapped "very near to," but not on, internal matrix surfaces. We can also suggest that the broad featureless "460 nm" absorption observed in Na/Rg matrices may be the blue shifted singlet component of a doublet plus singlet type absorption of Na atoms trapped in a site with a strong axial static asymmetry. Such a structure was previously proposed⁴⁶ to explain the reversible photobleaching phenomena associated with the 460 nm feature.

Our results also permit us to comment on the various previously proposed models of the spectra of S→P transitions of M/Rg systems. Essentially: the arguments we presented above in the Background section appear to have been borne out. The basic approach of treating the excitations as tightly bound Frenkel excitons in general, and as matrix perturbed excited metal atom states in particular, appears sound. Our model includes aspects of both the static crystal field, and dynamic J-T effect models, but rejects the importance of large external S-O modification effects on the electronic spectra of light metal atoms. We prefer the MC simulation approach to previously used analytical theoretical methods since it allows us to make fewer assumptions about the type and form of the results, and eliminates several opportunities to introduce human biases into the calculations.

C. Limitations of the Present Model

The lack of quantitative agreement between the results of our simulations and matrix experiments prompts us to examine our model for inherent deficiencies and possible improvements. We believe that the Semiclassical Franck-Condon Principle lineshape expression, Eq. 13, can yield quantitatively correct absorption spectra, provided the availability of accurate methods for calculating the initial state probability distribution, $P_i(Q)$, and the excited state energies, $E_f(Q)$. This is in spite of the neglect of the dynamical aspects of the Jahn-Teller problem imposed by the reflection approximation, and of the questionable assumption of Born-Oppenheimer separability near electronically degenerate nuclear configurations.

In our model we incorporate a classical method for generating and integrating over the initial state nuclear coordinate probability distribution. Even for the Na/Ar matrix systems, this method somewhat underpredicts the extent of geometry fluctuations away from the equilibrium structures. As the absorption data in Fig. 14 and Table 5 show, at the expense of introducing the simulation temperature as an adjustable parameter into our model, we could have achieved better cosmetic agreement with the observed peak splittings by running our simulations at higher temperatures, claiming to be compensating for this error. The incorporation of a quantum statistical mechanical method for calculating $P_i(Q)$ should alleviate this problem, and generalize the applicability of our approach to even lighter matrix systems.

Our adaptation of B&W's method for calculating the excited state energies has the compelling practical advantages of being conceptually simple and extremely fast from a computational standpoint. However, in part due to its simplicity, it suffers from an inability to account for several potentially important effects. Most distressing is the absence of even a "particle in a box" level treatment of the energy shifts caused by confining the M atom

valence electron in tight trapping sites. Our expression for the shift of the centroid of the absorption band depends only on the absolute distances between the M and Rg atoms, and is completely independent of the angular orientations (*e.g.*, open vs. closed structures) of the Rg atoms. The only contribution to the confinement energy comes from the repulsive parts of the Na-Ar excited state pair potentials. We believe that this deficiency is responsible for the model's consistent underprediction of the blue shifts of the absorption band centroids. Another important limitation of the B&W model is the use of only first-order perturbation theory and the minimum $\{p_{-1}, p_0, p_1\}$ basis set. This approach neglects any possible mixing of the p-states with other Na atom electronic states, and thus cannot reproduce the spatial distortions of the valence electron excited state probability distribution observed in other Na/Rg calculations⁷⁴. We are presently investigating alternatives to the original B&W formalism, including higher order perturbation theories and larger M^* atomic basis sets.

Our omission of spin limits the applicability of our model to $S \rightarrow P$ transitions of M atoms for which the magnitude of the intrinsic S-O splitting of the excited p-states is smaller than a few tens of wavenumbers. In matrix absorption spectra of $^2S \rightarrow ^2P$ transitions of heavy M atoms (*e.g.*, Cs, Ag, Au) the splitting between the observed doublet plus singlet components is due to the intrinsic S-O splitting of the M atom. We caution the reader here not to confuse the doublet plus singlet lineshapes generated in some of our Na/Ar simulations with these observations from heavy M atoms matrices. We are currently working on the inclusion of S-O coupling effects into our model by expanding the basis set to the six 2P_j spinorbitals and including a term for the intrinsic M atom S-O coupling in our valence electron Hamiltonian. We hope that this approach will also ultimately lead to a method for simulating the magnetic circular dichroism (MCD) spectra of matrix isolated M atoms.

VII. CONCLUSIONS

We have developed a method for calculating the relaxed structures, and optical absorption spectra of $S \rightarrow P$ transitions, of M/Rg systems. The model is based on a combination of the classical MC method and a simple first-order perturbation theory treatment of the excited M^* states, and as such is computationally very fast, but yields only qualitatively correct results.

We have applied this method to the specific cases of Na/Ar clusters, surfaces, and solid phase systems. The minimum energy structures for Na/Ar systems consist of approximately close-packed Ar atoms with a surface Na atom. If the Na atom is constrained to remain in the Ar bulk, it can be accommodated in as small a site as a single substitutional vacancy, resulting in minor radial distortions of the Ar surroundings. A Na atom is readily

accommodated in a four-atom substitutional site with negligible distortion of the Ar lattice. Trapping sites of high static symmetry yield the well known triplet absorption lineshape observed in the spectra of matrix isolated light alkali atoms. Na atoms in Ar clusters, on Ar surfaces, or in matrix trapping sites with a strong axial asymmetry result in a double plus singlet absorption lineshape. We have identified several deficiencies in our model in its present form, and are actively pursuing improvements.

We hope that these results will contribute to the ongoing effort¹⁰⁸⁻¹¹⁰ to explain the structures and photodynamics of light atoms in solid hydrogen.

VIII. FUTURE PLANS

We have begun to perform simulations of emission spectra from excited state Na* atoms in relaxed trapping site structures. We use the B&W formalism for calculating the Na* atom energies and treat the lowest energy as a point on an adiabatic potential energy surface on which we perform the MC simulation. Our preliminary results show strongly Stokes shifted emissions, and strong local lattice distortions which may be loosely interpreted as "NaAr_n exciplex formation." We will also soon begin simulations of the optical absorption spectra of Na atoms in liquid and random close-packed solid Ar, in support of an in-house effort to observe these absorptions experimentally. We will report all of these results elsewhere upon their completion.

REFERENCES

1. Proceedings of the High Energy Density Matter (HEDM) Conference, April 1992, edited by M.R. Berman (USAF Office of Scientific Research, Bolling AFB, DC, 1992).
2. P.G. Carrick, Specific Impulse Calculations of High Energy Density Solid Cryogenic Rocket Propellants. I: Atoms in Solid H₂, PL-TR-93-3014 (Phillips Laboratory, Edwards AFB, CA, 1993), also revised and submitted to the AIAA Journal of Propulsion and Power.
3. M. McCarty and G.W. Robinson, *Mol. Phys.* **2**, 415 (1959).
4. W. Weyhmann and F.M. Pipkin, *Phys. Rev.* **137**, A490 (1965).
5. B. Meyer, *J. Chem. Phys.* **43**, 2986 (1965).
6. R.B. Merrithew, G.V. Marusak, C.E. Blount, *J. Mol. Spec.* **29**, 54 (1969).
7. L.C. Balling, M.D. Havey, J.F. Dawson, *J. Chem. Phys.* **69**, 1670 (1978).
8. M. Hofmann, S. Leutwyler, and W. Schulze, *Chem. Phys.* **40**, 145 (1979).
9. T. Welker and T.P. Martin, *J. Chem. Phys.* **70**, 5683 (1979).
10. J. Hormes and B. Karrasch, *Chem. Phys.* **70**, 29 (1982).
11. J. Hormes and J. Schiller, *Chem. Phys.* **74**, 433 (1983).
12. J. Rose, D. Smith, B.E. Williamson, P.N. Schatz, and M.C.M. O'Brien, *J. Phys. Chem.* **90**, 2608 (1986).
13. M.E. Fajardo, P.G. Carrick, and J.W. Kenney III, *J. Chem. Phys.* **94**, 5812 (1991).
14. S. Tam and M.E. Fajardo, *J. Chem. Phys.* **99**, 854 (1993).
15. R.E. Smalley, D.A. Auerbach, P.S.H. Fitch, D.H. Levy, and L. Wharton, *J. Chem. Phys.* **66**, 3778 (1977).
16. R.P. Saxon, R.E. Olson, and B. Liu, *J. Chem. Phys.* **67**, 2692 (1977).
17. J. Tellinghuisen, A. Ragone, M.S. Kim, D.J. Auerbach, R.E. Smalley, L. Wharton, and D.H. Levy, *J. Chem. Phys.* **71**, 1283 (1979).

18. G. Aepfelbach, A. Nunnemann, and D. Zimmermann, Chem. Phys. Lett. **96**, 311 (1983).
19. R. Duren, W. Groger, E. Hasselbrink, and R. Liedtke, J. Chem. Phys. **74**, 6806 (1981).
20. F. Van Den Berg, R Morgenstern, and C.Th.J. Alkemade, Chem. Phys. **93**, 171 (1985).
21. R.A. Aziz and M.J. Slaman, Mol. Phys. **58**, 679 (1986).
22. J.A. Boatz and M.E. Fajardo, "Monte Carlo Simulations of the Structures and Optical Absorption Spectra of Na/Ar Clusters and Solids," in reference 1.
23. M.E. Fajardo, J. Chem. Phys. **98**, 110 (1993).
24. A.A. Belyaeva, Yu.B. Predtechenskii, and L.D. Shcherba, Opt. Spektrosk. (Engl. Transl.) **24**, 233 (1968).
25. M. Brith and O. Schnepf, J. Chem. Phys. **39**, 2714 (1963).
26. S.L. Kupferman and F.M. Pipkin, Phys. Rev. **166**, 207 (1968).
27. J.E. Francis, Jr. and S.E. Webber, J. Chem. Phys. **56**, 5879 (1972).
28. F. Forstmann, D.M. Kolb, D. Leutloff, and W. Schulze, J. Chem. Phys. **66**, 2806 (1977).
29. A.A. Belyaeva, Yu.B. Predtechenskii, and L.D. Shcherba, Opt. Spektrosk. (Engl. Transl.) **34**, 21 (1973).
30. R.L. Mowery, J.C. Miller, E.R. Krausz, P.N. Schatz, S.M. Jacobs, and L. Andrews, J. Chem. Phys. **70**, 3920 (1979).
31. H. Kuppelmaier, H.J. Stockmann, A. Steinmetz, E. Gorlach, and H. Ackermann, Phys. Lett. **98A**, 187 (1983).
32. K.S. Song and C.H. Leung, Solid State Comm. **57**, 129 (1986).
33. I.Ya. Fugol, A.M. Ratner, and E.M. Yurtaeva, Phys. Stat. Sol. B **160**, 245 (1990).
34. P.A. Lund, D. Smith, S.M. Jacobs, and P.N. Schatz, J. Phys. Chem. **88**, 31 (1984).
35. H.J. Stockmann, Z. Phys. B **54**, 229 (1984).

36. M. Vala, K. Zeringue, J. ShakhEmampour, J. Rivoal, and R. Pyzalski, *J. Chem. Phys.* **80**, 2401 (1984).
37. M.C.M. O'Brien, *J. Chem. Phys.* **82**, 3870 (1985).
38. M.C.M. O'Brien, *J. Phys. C* **18**, 4963 (1985).
39. C. Samet, J.L. Rose, B.E. Williamson, and P.N. Schatz, *Chem. Phys. Lett.* **142**, 557 (1987).
40. R. Pellow and M. Vala, *J. Chem. Phys.* **90**, 5612 (1989).
41. M. Moskovits and J.E. Hulse, *J. Chem. Phys.* **67**, 4271 (1977).
42. A. Schrimpf, R. Rosendahl, T. Bornemann, H.J. Stockmann, F. Faller, and L. Manceron, *J. Chem. Phys.* **96**, 7992 (1992).
43. M. Lax, *J. Chem. Phys.* **20**, 1752 (1952).
44. P.R. Moran, *Phys. Rev.*, **137A**, 1016 (1965).
45. C. Crepin and A. Tramer, *J. Chem. Phys.* **97**, 4772 (1992).
46. L.C. Balling, J.F. Dawson, M.D. Havey, and J.J. Wright, *Phys. Rev. Lett.*, **43**, 435 (1979).
47. J.F. Dawson and L.C. Balling, *J. Chem. Phys.* **71**, 836 (1979).
48. F. Forstmann and S. Ossicini, *J. Chem. Phys.* **73**, 5997 (1980).
49. S. Ossicini and F. Forstmann, *J. Chem. Phys.* **75**, 2076 (1981).
50. S. Ossicini and F. Forstmann, *Nuovo Cimento Soc. Ital. Fis.* **1D**, 688 (1982).
51. L.C. Balling and J.J. Wright, *J. Chem. Phys.* **79**, 2941 (1983).
52. L.C. Balling and J.J. Wright, *J. Chem. Phys.* **81**, 675 (1984).
53. M.E. Fajardo, *J. Chem. Phys.* **98**, 119 (1993).
54. C. Kittel, Introduction to Solid State Physics, 6th edition (Wiley, New York, 1986).
55. N. Schwentner, E.E. Koch, and J. Jortner, Electronic Excitations in Condensed Rare Gases (Springer-Verlag, Berlin, 1985).
56. J. Hormes, *Chem. Phys. Lett.* **112**, 431 (1984).
57. N. Schwentner and M. Chergui, *J. Chem. Phys.* **85**, 3458 (1986).

58. J. Mort, F. Luty, and F.C. Brown, *Phys. Rev.* **137**, A566 (1965).
59. D.Y. Smith, *Phys. Rev.* **137**, A574 (1965).
60. C.H. Henry, S.E. Schnatterly, and C.P. Slichter, *Phys. Rev.* **137**, A583 (1965).
61. G.A. Osborne and P.J. Stephens, *J. Chem. Phys.* **56**, 609 (1972).
62. K. Cho, *J. Phys. Soc. Japan*, **25**, 1372 (1968).
63. P.H. Yuster and C.J. Delbecq, *J. Chem. Phys.* **21**, 892 (1953).
64. Y. Toyozawa and M. Inoue, *J. Phys. Soc. Japan* **21**, 1663 (1966).
65. A. Jablonski, *Phys. Rev.* **68**, 78 (1945).
66. R.P. Futrelle, *Phys. Rev. A* **5**, 2162 (1972).
67. W.E. Baylis, *J. Phys. B* **10**, L477 (1977).
68. W.P. West, P. Shuker, and A. Gallagher, *J. Chem. Phys.* **68**, 3864 (1978).
69. K.M. Sando, G.J. Erickson, and R.C. Binning Jr., *J. Phys. B* **12**, 2697 (1979).
70. G.J. Erickson and K.M. Sando, *Phys. Rev. A* **22**, 1500 (1980).
71. R.H.G. Reid and A. Dalgarno, *Phys. Rev. Lett.* **22**, 1029 (1969).
72. C.H. Becker, P. Casavecchia, Y.T. Lee, R.E. Olson, and W.A. Lester Jr., *J. Chem. Phys.* **70**, 5477 (1979).
73. V. Aquilanti and G. Grossi, *J. Chem. Phys.* **73**, 1165 (1980).
74. C. Tsou, D.A. Estrin, and S.J. Singer, *J. Chem. Phys.* **93**, 7187 (1990).
75. D.A. Estrin, C. Tsou, and S.J. Singer, *Chem. Phys. Lett.* **184**, 571 (1991).
76. C. Tsou, D.A. Estrin, and S.J. Singer, *J. Chem. Phys.* **96**, 7977 (1992).
77. G. Martyna, C. Cheng, and M.L. Klein, *J. Chem. Phys.* **95**, 1318 (1991).
78. K. Haug and H. Metiu, *J. Chem. Phys.* **95**, 5670 (1991).
79. J.P. Visticot, P. de Pujo, J.M. Mestdagh, A. Lallement, J. Berlande, O. Sublemontier, P. Meynadier, and J. Cuvellier, *J. Chem. Phys.* **100**, 158 (1994).
80. D. Eichenauer and R.J. LeRoy, *J. Chem. Phys.* **88**, 2898 (1988).
81. L. Perera and F.G. Amar, *J. Chem. Phys.* **93**, 4884 (1990).

82. X.J. Gu, D.J. Levandier, B. Zhang, G. Scoles, and D. Zhuang, *J. Chem. Phys.* **93**, 4898 (1990).
83. M. Kmetc and R.J. LeRoy, *J. Chem. Phys.* **95**, 6271 (1991).
84. R.G. Gordon, *Adv. Mag. Resonance* **3**, 1 (1968).
85. D.A. McQuarrie, Statistical Mechanics (Harper & Row, New York, 1976).
86. G. Herzberg, Molecular Spectra and Molecular Structure I. Spectra of Diatomic Molecules (Van Nostrand Reinhold, New York, 1950).
87. E.A. Gislason, *J. Chem. Phys.* **58**, 3702 (1973).
88. E.J. Heller, *J. Chem. Phys.* **68**, 2066 (1978).
89. S.Y. Lee, *J. Chem. Phys.* **82**, 4588 (1985).
90. M.E. Fajardo and V.A. Apkarian, *J. Chem. Phys.* **89**, 4102 (1988).
91. V.A. Apkarian, private communication (1993).
92. C. Cohen-Tannoudji, B. Diu, and F. Laloe, Quantum Mechanics Vol. II (Wiley, New York, 1977) see appendix II.
93. W.G. Lawrence and V.A. Apkarian, to be published.
94. D. Maillard, J. Fournier, H.H. Mohammed, and C. Giradet, *J. Chem. Phys.* **78**, 5480 (1983).
95. G. Arfken, Mathematical Methods for Physicists (Academic, New York, 1970).
96. R.N. Zare, Angular Momentum (Wiley, New York, 1988).
97. N. Metropolis, A.W. Rosenbluth, M.N. Rosenbluth, A.H. Teller, and E. Teller, *J. Chem. Phys.*, **21**, 1087 (1953).
98. T.G. Gibbons and M.L. Klein, *J. Chem. Phys.* **60**, 112 (1974).
99. P. Korpiun and E. Luscher, in Rare Gas Solids Volume II, edited by M.L. Klein and J.A. Venables (Academic, London, 1976).
100. M.P. Allen and D.J. Tildesley, Computer Simulations of Liquids, (Oxford, New York, 1990).

101. C.E. Moore, Atomic Energy Levels Volume I, (NSRDS-NBS 35, Washington DC, 1971).
102. J.W. Cooley, *Math. Computation* **XV**, 363 (1961).
103. J.K. Cashion, *J. Chem. Phys.* **39**, 1872 (1963).
104. N. Kestner and N. Brenner, private communication (1991).
105. I.L. Garzon, X.P. Long, R. Kawai, and J.H. Weare, *Chem. Phys. Lett.* **158**, 525 (1989).
106. H.R. Glyde, in Rare Gas Solids Volume I, edited by M.L. Klein and J.A. Venables (Academic, London, 1976).
107. V.V. Goldman, *Phys. Rev.* **174**, 1041 (1968).
108. D. Li and G.A. Voth, *J. Chem. Phys.*, **96**, 5340 (1992).
109. D. Scharf, G.J. Martyna, D. Li, G.A. Voth, and M.L. Klein, "Nature of the trapping sites and electronic spectrum of lithium atoms in the quantum solids para-hydrogen and ortho-deuterium," in Proceedings of the High Energy Density Matter (HEDM) Conference, 1993, edited by T. Thompson, PL-TR-93-3041, (USAF Phillips Laboratory, Edwards AFB, CA 1993).
110. R.B. Gerber, Z. Li, and A.B. McCoy "Vibrational Dynamics of Quantum Clusters and Solids," in Proceedings of the High Energy Density Matter (HEDM) Conference, 1993, edited by T. Thompson, PL-TR-93-3041, (USAF Phillips Laboratory, Edwards AFB, CA 1993).